



HAL
open science

C-STEM: ENGINEERING NICHE-LIKE MICRO-COMPARTMENTS FOR OPTIMAL AND SCALE-INDEPENDENT EXPANSION OF HUMAN PLURIPOTENT STEM CELLS IN BIOREACTORS

Philippe J.R. Cohen, Elisa Luquet, Justine Pletenka, Andrea Leonard, Elise Warter, Basile Gurchenkov, Jessica Carrere, Clement Rieu, Jerome Hardouin, Fabien Moncaubeig, et al.

► **To cite this version:**

Philippe J.R. Cohen, Elisa Luquet, Justine Pletenka, Andrea Leonard, Elise Warter, et al.. C-STEM: ENGINEERING NICHE-LIKE MICRO-COMPARTMENTS FOR OPTIMAL AND SCALE-INDEPENDENT EXPANSION OF HUMAN PLURIPOTENT STEM CELLS IN BIOREACTORS. 2021. hal-03396261

HAL Id: hal-03396261

<https://hal.science/hal-03396261v1>

Preprint submitted on 22 Oct 2021

HAL is a multi-disciplinary open access archive for the deposit and dissemination of scientific research documents, whether they are published or not. The documents may come from teaching and research institutions in France or abroad, or from public or private research centers.

L'archive ouverte pluridisciplinaire **HAL**, est destinée au dépôt et à la diffusion de documents scientifiques de niveau recherche, publiés ou non, émanant des établissements d'enseignement et de recherche français ou étrangers, des laboratoires publics ou privés.

1 **TITLE** : C-STEM: ENGINEERING NICHE-LIKE MICRO-COMPARTMENTS FOR OPTIMAL
2 AND SCALE-INDEPENDENT EXPANSION OF HUMAN PLURIPOTENT STEM CELLS IN
3 BIOREACTORS

4
5 **Short title** : Scale-independent expansion of biomimetic hPSC colonies

6
7 **AUTHORS**

8 Philippe J.R. Cohen*^{1,2}, Elisa Luquet², Justine Pletenka², Andrea Leonard², Elise Warter², Basile Gurchenkov³,
9 Jessica Carrere², Clément Rieu², Jerome Hardouin², Fabien Moncaubeig², Michael Lanero², Eddy Quelennec^{1,2},
10 Helene Wurtz², Emilie Jamet², Maelle Demarco², Celine Banal¹, Paul Van Liedekerke⁴, Pierre Nassoy^{5,6}, Maxime
11 Feyeux², Nathalie Lefort^{‡1}, Kevin Alessandri^{‡2}

12
13 **AFFILIATIONS**

14 1 Université de Paris, Imagine Institute, iPSC Core Facility, INSERM UMR U1163, F-75015 Paris, France

15 2 Treefrog Therapeutics, F-33600 Pessac, France

16 3 Paris Brain Institute, ICM Paris, F-75013 Paris, France

17 4 Inria Paris & Sorbonne Université LJLL, 2 Rue Simone IFF, F-75012, Paris, France

18 5 LP2N, Laboratoire Photonique Numérique et Nanosciences, Univ. Bordeaux, F-33400 Talence, France

19 6 Institut d'Optique Graduate School & CNRS UMR 5298, F-33400 Talence, France

20 ‡ These authors contributed equally to this work.

21 * Corresponding author: Philippe J.R. Cohen philippe.cohen@treefrog.fr

22 **ABSTRACT**

23 Human pluripotent stem cells (hPSCs) have emerged as the most promising cellular source for cell therapies. To
24 overcome scale up limitations of classical 2D culture systems, suspension cultures have been developed to meet
25 the need of large-scale culture in regenerative medicine. Despite constant improvements, current protocols relying
26 on the generation of micro-carriers or cell aggregates only achieve moderate amplification performance. Here,
27 guided by reports showing that hPSCs can self-organize *in vitro* into cysts reminiscent of the epiblast stage in
28 embryo development, we developed a physio-mimetic approach for hPSC culture. We engineered stem cell niche
29 microenvironments inside microfluidics-assisted core-shell microcapsules. We demonstrate that lumenized three-
30 dimensional colonies maximize viability and expansion rates while maintaining pluripotency. By optimizing
31 capsule size and culture conditions, we scale-up this method to industrial scale stirred tank bioreactors and
32 achieve an unprecedented hPSC amplification rate of 282-fold in 6.5 days.

33

34 **TEASER**

35 Optimizing human pluripotent stem cells amplification by recapitulating and protecting biomimetic colonies in a
36 bioreactor

37 **INTRODUCTION**

38

39 Following pioneering works targeting Parkinson's disease (1, 2), diabetes (3, 4), macular degeneration (5) or heart
40 failure (6, 7), cell therapies are now addressing an increasing diversity of indications (8, 9). Therapeutic cells
41 represent a hope for millions of patients worldwide with chronic diseases or unmet medical needs. For each of
42 those patients, the number of required cells range between 10^5 and 10^{10} cells. While academic pre-clinical studies
43 or small-scale clinical trials have already been proved to be successful, a transition to true clinical scale is now
44 urgently needed. To enable treatment of thousands to millions of patients, production capacity must scale while
45 maintaining high-quality cells compatible with transplantation.

46 Due to their unlimited self-renewal capacity and potency to give rise to any cell type in the body, human
47 pluripotent stem cells (hPSCs) hold great promise to provide the required quantities of therapeutic cells. *In vivo*, a
48 few embryonic stem cells can give rise to the 30×10^{12} cells of the adult human body (10) while maintaining their
49 genome integrity. As a consequence, much effort has been dedicated to the isolation and *in vitro* culture of these
50 cells in physiological conditions.

51 Historically, the first stem cell lines were established by micro-dissecting embryos and manual passaging as two-
52 dimensional (2D) adherent epithelial colonies on a layer of feeder cells (11–13). Cell proliferation and
53 pluripotency maintenance were thus achieved *in vitro*. The need for an embryonic source was then alleviated with
54 the discovery that differentiated cells could be reprogrammed into induced pluripotent stem cells (iPSC) (14).
55 This breakthrough led to pioneer works in developmental cell biology and catalyzed the development of cell
56 therapy applications. Even though a lot of work has been devoted to the development of media and substrate
57 compatible with clinical use, topology of hiPSCs cultures has not been gathering the same attention. Nevertheless,
58 2D *in vitro* cultures suffer high mortality rates, spontaneous differentiation and genetic drift (15). An estimated
59 40-fold increase in the number of mutations compared to *in vivo* conditions (16) often results in rejection of
60 clinical batches due to safety concerns (17, 18). In addition, 2D culture systems have limited “scale-out”
61 possibilities: for example, generating 1 trillion pluripotent stem cells, would require almost 1000 m² of plastic

62 dishes and countless handmade passaging (15). The non-scalability and the inability to conserve high quality cells
63 remain the main limitations of 2D culture systems for clinical applications (18).

64 More recently, 3D hPSCs cultures have been developed to model developmental processes. After seeding stem
65 cells in bulk extracellular matrix (ECM) (19, 20) or using microfluidic chips (21), cell clusters self-organize into a
66 monolayered epithelium recapitulating numerous features of an epiblast that generates *in vivo* all tissues in an
67 amniote embryo through gastrulation. Even though these elegant approaches allowed to gain much insight into
68 morphogenesis mechanisms (22), they are not designed for the production of hPSCs per se.

69 From a bioproduction perspective, significant advances have been achieved by developing 3D suspension cultures
70 and bioreactors. Whether hPSCs are grown as floating aggregates or adherent at the surface of microcarriers,
71 those systems provide increased surface-to-volume ratio and scale-up potentialities. Additionally, the use of
72 stirred-tank bioreactors (STBR) allowed better control of the culture parameters without direct human
73 intervention. Indeed, stirring-mediated mechanical agitation avoids sedimentation of the aggregates or
74 microcarriers onto the bottom of the culture vessel and heterogeneities in the culture medium compositions.
75 Nonetheless, one intrinsic drawback of agitation is that hydrodynamic shear induces cellular damages (23). This
76 effect is all the more dramatic as the vessel increases in size: the larger the volume of the bioreactor is, the more
77 power per unit of volume needs to be injected for effective homogenization. Even though expansion rates with
78 hPSC aggregates are regularly increased and could reach up to 70-fold within 7 days (24, 25), the ability of
79 scaling up the volume of the production is still restricted. Typically, this mechanical upper limit makes it difficult
80 to reach batches larger than 1 liter or equivalently few billion cells. Finally, the current bottleneck for industrial
81 scalability is the difficulty to fulfill simultaneously high amplification rate, volume and physiological quality.

82 In this work, by bridging the gap between two distinct communities, namely developmental biology and stem
83 cells bioprocessing, we show that recapitulation of hPSC niche-like micro-environments allows to optimize the
84 suspension culture of hPSC in STBRs. More precisely, we propose a system that utilizes a high throughput
85 microfluidic encapsulation technology compatible with suspension culture of stem cells in a bioreactor and
86 amenable to the production of large volume batches without any degradation of cell survival in contrast with 2D
87 colony-based systems for instance. Briefly, iPSCs are encapsulated in alginate hollow microcapsules internally

88 coated with ECM components at low cell seeding concentration. We assess the maintenance of stemness and
89 pluripotency upon 3D culture in suspension. We then characterize the cell growth inside the capsules before
90 showing that upscaling to 10 liter stirred-tank bioreactor allows to reach unrivalled amplification factors.
91 Altogether, the C-STEM technology overcomes the scale-up bottleneck faced in cell therapy bioproduction. We
92 discuss that the origins of this performance could be related to unprecedented cell viability of 3D lumenized
93 colonies within these capsules.

94

95 **RESULTS**

96 **High-throughput microfluidic encapsulation of hiPSCs**

97 Using a microfluidic technique to generate hollow hydrogel spheres (Fig. 1A, Movie S1, and detailed description
98 in the Materials and Methods section) previously developed by us and others (26–29) we encapsulated human
99 induced pluripotent stem cells (hiPSC) in liquid core capsules. Briefly, the working principle is the following: a
100 three-layered cylindrical flow is generated using a co-extrusion microfluidic device: the cell suspension is
101 surrounded by an alginate solution. Both solutions are separated by a sorbitol solution to prevent diffusion of
102 calcium released from the cell suspension towards the alginate solution. Upon exiting the microfluidic device at
103 high flow rate (on the order of 120 ml/h for all three solutions), the liquid jet is fragmented into small droplets
104 due to the Plateau-Rayleigh instability. By contrast with the dripping regime obtained at lower flow rate that gives
105 rise to droplets of size in the order of the capillary length (i.e. ~mm), the droplet radius is here dictated by the
106 extruder's nozzle size (~200 microns diameter) (30). This reduced size, which is below the distance over which
107 oxygen and nutrients supply is limited within a tissue, allows to avoid the formation of a necrotic core (31). Once
108 they fall in a calcium bath, the alginate solution droplets undergo gelation and trap the cell suspension in their
109 interior. Our routine protocol produces capsules at a rate of about 3 kHz (Fig. S1), meaning that a 30 seconds
110 operation generates 100,000 capsules. Morphological analysis shows that capsules are monodisperse in size with
111 mean external radius $R = 205 \mu\text{m} \pm 39 \mu\text{m}$. and that their shape is close to spherical, with a circularity parameter
112 $C = 0.84 \pm 0.04$ (Fig. 1B).

113 In order to provide a niche-like environment to hiPSCs, Matrigel, an ECM mixture, is co-injected with the cell
114 suspension (28). Empirically, we found that a minimal volume fraction of 25% was required to form a continuous
115 matrix layer anchored to the inner wall of the capsule, with the excess (if any) being found as floating gel pieces
116 inside the capsule (29). Most of the experiments reported in these works were performed with 50% of Matrigel in
117 volume fraction. The granularity seen in the core of the capsule (Fig. 1E) thus corresponds to small floating
118 aggregates of ECM. Most encapsulations reported hereafter were performed with a density of 0.4×10^6 cells/ml in
119 the cell/matrix suspension, unless otherwise stated, and led to a mean number of cells per capsule right after
120 encapsulation (day 0) of ~ 2.5 (Fig. 1C), meaning that $\sim 10\%$ of the capsules are empty, consistently with a Poisson
121 distribution. After 6 to 7 days of culture, practically defined as the harvest time under these seeding conditions, 3D
122 colonies of hiPSCs were observed, suggesting, not only that hiPSCs survive, but also that they could proliferate
123 (Fig. 1D). Higher magnification reveals the presence of a lumen (Fig. 1E).

124

125 **Culture, expansion and stemness of encapsulated 3D hiPSC colonies**

126 Using phase contrast imaging, we observed in more details the growth kinetics of these 3D hiPSC colonies. First,
127 hiPSCs form a small cluster (typically during the first 24h) before self-organizing in a cyst structure around a
128 central lumen (Fig. 2A, Movie S2 & S3). Then, the 3D hiPSC colonies grow within the capsules while keeping
129 the same spherical shape. In the early stages, the cells within the monolayer of the cyst have a cuboid cell shape of
130 about $10 \mu\text{m}$ side (Fig. 2B left, ~ 5 days post-encapsulation). Before harvesting, as seen in the confocal image of a
131 representative 7 day-old hiPSC 3D colony immunostained for actin and nucleus, cells exhibit an elongated
132 morphology perpendicular to the surface of the cyst. Yet, the cyst remains monolayered suggesting a transition
133 towards a pseudostratified columnar epithelium with most nuclei being located on the basal side opposing the
134 lumen. In this stage, the cysts are characterized by a thickness of about $\sim 40 \mu\text{m}$ (Fig. 2B right) and a radius of
135 about $\sim 100 \mu\text{m}$ (Fig. S2, day 7). Note that later stages are ignored. Indeed, if cells are not harvested, cysts become
136 confined by the capsules and further grow inwards leading to a progressive loss of the lumen (Movie S4) and
137 eventually the appearance of “fractures” (Fig S2).

138 The maintenance of the stemness of the encapsulated 3D hiPSC colonies was then checked. The expression of key
139 self-renewal markers such as OCT4 and SOX2 was first assessed after capsule dissolution, fixation and staining.
140 The alginate shell was dissolved by adapting the protocol of (29): we performed a short rinse of ReLeSR, which
141 serves here as a calcium chelator that gently dissolves the alginate gel. Fixation and immunostaining were carried
142 out following standard protocols (see Materials and Methods section) while preserving the 3D architecture. Image
143 analysis of representative confocal images of individual cysts (Fig. 2C (top row) and Fig. S2) allows to derive that
144 the percentage of cells positive for OCT4 and SOX2 is 97% (Fig. 2D top row). To further assess the consistency
145 of stemness phenotype, we applied the approach pursued in a different context for epiblast-stage hPSCs spheroids
146 by Freedman et al. (32). “Naked” hiPSCs cysts were dissociated and replated into 2D cultures (Fig. 2C). We
147 observed that 2D colonies are readily formed and stemness markers are detected (Fig. 2C-D, bottom row) with a
148 percentage of OCT4 and SOX2 positive cells larger than 98%.

149 Following this characterization at the scale of individual capsules, we sought to assess the potential variability
150 between capsules and between hiPSC lines. We thus dissociated the bulk suspension cultures, extended staining to
151 OCT4, SOX2 and NANOG and performed flow cytometry (Fig. 2E-F). For 4 different cell lines (see Materials
152 and Methods section) by pooling all experiments (n = 42) of each hiPSC line, we found that the mean percentage
153 of positive cells is 93% OCT4, 98% SOX2 and 92% NANOG (Fig. 2F). This finding is in good agreement with
154 the above-described findings at the single 3D colony level, suggesting an overall homogeneity of the stem cell
155 culture.

156 Note that, if capsules culture was prolonged beyond 7 days, despite drastic changes of topology from cyst to
157 aggregate (Fig. S2 C-E and Movie S4), the stemness of the hiPSCs was not affected, as revealed by OCT4 and
158 SOX2 staining before and after lumen collapse (Fig. S2 B-C), suggesting that harvest timing is not critically
159 stringent with respect to the stemness maintenance.

160

161 **Pluripotency and genomic integrity of encapsulated 3D hiPSC colonies**

162 While OCT4, SOX2 and NANOG are often considered as pluripotency markers, they actually are stemness
163 markers. To assess more thoroughly the pluripotency and validate the quality of hPSCs upon 3D culture in their

164 ability to differentiate as bona fide pluripotent stem cells, the most commonly used assay is the trilineage
165 differentiation assay (33), in which stochastic differentiation is induced. Following a standard protocol (34) (see
166 Materials and Methods section), decapsulated and dissociated hiPSC (from the three available cell lines) were
167 driven towards early differentiation, as shown by the stainings for specific markers of the 3 germ layers: namely
168 β -tubulin (TUJ1) for ectoderm, smooth muscle actin (α -SMA) for mesoderm and α -fetoprotein (AFP) for
169 endoderm (Fig. 3A). Even though the expression level may differ from one cell line to another, all stainings are
170 positive and clearly reveal a differentiation into the three germ layers.

171 To further quantify the differentiation potential after 3D culture within capsules, we used qPCR Scorecard™
172 assay to evaluate the transcription profile of the cells obtained in the trilineage assay (Fig. 3B). The set of 94
173 previously validated qPCR markers of self-renewal, ectoderm, mesendoderm, mesoderm and endoderm (35, 36)
174 was used to compare standard 2D culture and 3D culture-in-capsules. Fig. 3B shows that, for a given marker and
175 a given cell line, there is a striking similarity between the transcription signatures in 2D and 3D culture
176 conditions, indicating that pluripotency assessed as the *in vitro* differentiation capability of hiPSC clones is
177 definitely not altered in our encapsulated 3D colonies. A pooled analysis by germ layer (Fig. S4) confirms similar
178 differentiation profile between 2D and 3D stem cells.

179 Finally, to control genomic integrity of the 3D colonies, we performed high resolution SNP (single nucleotide
180 polymorphism) arrays before and after amplification within the capsules (Fig. 3C and Fig. S5) (37). Comparative
181 SNP analysis showed the absence of aneuploidies, deletions or duplications, as evidenced by the superimposable
182 karyotypes. The high degree of SNP concordance (>99.8% for all hiPSC lines) before and after encapsulation
183 confirms cell line identity (Fig. 3D).

184

185 **Comparative growth of 3D hiPSC colonies at the scale of a single capsule, in a static suspension and in** 186 **bioreactors**

187 To evaluate whether the strategy to produce 3D colonies in ECM-coated capsules impacts the growth and
188 expansion rates of hiPSC, we performed a series of systematic experiments to probe the cell growth kinetics. The

189 standard 2D cell cultures were taken as a control. Since the amplification factor is defined as $AF=N(t_0+Dt)/N(t_0)$,
190 where $N(t_0)$ and $N(t_0+Dt)$ are the cell numbers at the initial time t_0 and t_0+Dt respectively, direct cell counting at
191 day 6 after passaging give a mean $AF_{2D}(t=6 \text{ days})\sim 13$. Since, by definition, $AF(Dt)=2^{Dt/PDT}$, with PDT the cell
192 population doubling time, by pooling amplification factors at different harvesting time, we obtain a mean
193 $PDT_{2D}=34h \pm 5$ hours for iPS C line, which falls within the range of data reported in the literature (14, 15, 38).

194 Then, in order to characterize the growth of individual encapsulated 3D hiPSC colonies, we cultured them in 35
195 mm petri dishes (typically as few as 10 capsules in a volume of medium ~ 5 ml, permitting to conserve the same
196 medium for the whole course of the experiment without any risk of nutrient depletion and acidification). We
197 performed time-lapse phase contrast imaging over a one-week period. We assume that cell volume remains
198 constant, which allows us to derive $AF_{capsule}(Dt)=V(t_0+Dt)/V(t_0)$ by measuring the volume of the cyst $V(t)$ from
199 image analysis: $V(t)=\frac{4\pi}{3}(R_{out}^3 - R_{in}^3)$, where R_{in} and R_{out} are the average internal and external radii of the cyst

200 (see notations on Fig. 4A). Figure 4B shows the evolution of $AF_{capsule}$ as a function of time for individual
201 encapsulated 3D colonies. One immediately observes that $AF_{capsule}(t=7 \text{ days})= 212$. Additionally, since AF
202 increases exponentially as $AF(\Delta t) = \exp\left(\frac{\ln 2 \cdot \Delta t}{PDT_{capsule}}\right)$, one finds $PDT_{capsule} = 22 \pm 1$ hours.

203 With the perspective of scaling up the production of hiPSCs, we also investigated how the growth of encapsulated
204 3D hiPSC colonies was impacted when cultured in conditions of i) static bulk suspension in standard T-Flasks
205 (Fig. 4B) and ii) stirred suspension in a benchtop bioreactor (Fig. 4C). STBRs are the most common bioreactors
206 used to culture biological agents for biotechnological applications. Besides their capacity to monitor and adjust the
207 pH and oxygen partial pressure and to refresh the medium, the mechanical agitation provided by the impellers
208 allows better fluid mixing and oxygen transfer ability as compared to static suspension (39). However, the
209 drawback may also be that the shear stress induced by the impellers was shown to cause deleterious effects such as
210 cell death or decrease in cell growth in aggregate- or microcarrier-based cultures (40, 41). Practically, we loaded
211 capsules from a same batch in T-flasks and in a STBR at the same initial density. The bioreactor impeller
212 rotational speed was set to 150 rpm, which is sufficient to maintain medium homogeneity and avoid capsule
213 sedimentation. We could not detect any change in the shape of the capsules and 3D colonies under these stirring

214 conditions. Then, after dissolution of the alginate shell and dissociation of the cysts, we counted the stem cells in
215 both static and stirred culture conditions to derive the amplification factors AF in time. We found $AF_{flask}(7\ days)=$
216 109 ± 6 and $AF_{bioreactor}(7\ days)= 104 \pm 18$ (Fig. 4D). From the values of the characteristic times for the
217 exponential variation of AF, we could calculate, as explained above, $PDT_{flask}= 25 \pm 6$ h and $PDT_{STBR}=25 \pm 3$ h (Fig.
218 4E). Three remarks can be made. First, these PDT values are significantly lower than the ones derived from 2D
219 cultures, indicating again that the expansion is greatly improved in 3D, as evidenced by the low number of dead
220 cells in capsules (Fig. 4F) as compared with 2D colonies (Fig. S6). Second, the AF values are about twice as low
221 as the one derived from the measurements at the single capsule level. Third, the absence of statistical difference
222 between the two culture systems suggests that, while the impeller-induced shear stress does not affect cell
223 viability, stirred suspension culture in a benchtop bioreactor with expected better homogenization does not
224 enhance the expansion under the experimental conditions selected here.

225 Additionally, we performed flow cytometry analysis and found that more than 92% of the cells are positive for
226 SOX2, NANOG and OCT4. Stemness thus remains high and similar between static and stirred cultures (Fig. S7),
227 indicating that, by contrast with previous reports (42), shear stress does not trigger the differentiation of hiPSC
228 colonies grown in hollow capsules. Finally, in order to confirm that the amplification factors reported above are
229 not hiPSC line specific, we carried out the same series of experiments for the other 3 cell lines in static culture
230 (Fig. 4E). Not only are the differences between cell lines not significant, but their PDT in 3D is also found very
231 close to the value derived for the commercial hiPSC line that we have extensively investigated in this section, i.e.
232 $PDT_{flask}= 27 \pm 2$ h by averaging over all 3 cell lines.

233 234 **Optimized culture conditions: Impact of capsule size and oxygen tension**

235 As shown above, the static or stirred batch cultures of hiPSC colonies in capsules yielded amplification at day 7
236 about twice as low as the one measured at the single capsule level. Although this difference only corresponds to a
237 3h difference in PDT, we sought to address this issue and find out solutions to further improve the amplification
238 of hiPSC in batch for large-scale production. We investigated the impact of two possible parameters.

239 First, we tested whether hiPSC amplification depends on the cell seeding density. The most obvious way would
240 be to increase the volume fraction of cells in the core solution loaded to the microfluidic injector. However, this
241 would lead to earlier and more frequent harvesting. Instead, we pursued a different strategy. We kept the cell
242 density constant but increased the size of the capsules by changing the size of the nozzle (28). Doing so, for a
243 given volume of the encapsulation cell suspension, the number of produced capsules is indeed reduced by
244 $(R_{big}/R_{small})^3$ but the mean number of cells per capsule, λ , is increased by the same fold. In the context of sparse
245 distribution, Poisson statistics applies and the generation of 300 μm in radius capsules instead of 200 μm leads to
246 an increase in λ by about 3 fold. The immediate consequence is that the probability to have capsules containing no
247 cell is decreased from about 8% to negligible ($\sim 0.03\%$). But, more importantly, the probability to have capsules
248 with only one cell that may die or exhibit some lag phase before proliferation goes from 20% to 0.3%. High
249 occurrence of capsules loaded with only one cell is expected to lower the effective amplification factor and thus to
250 increase the doubling time of the cell population. Fig. 5A shows representative phase contrast images of 300 μm
251 in radius capsules filled with hiPSC colonies. Noteworthy, most capsules contain several cysts, suggesting that
252 cyst growth was nucleated from several cell aggregates. More quantitatively, after monitoring the growth kinetics
253 in benchtop STBR, derivation of the time constant reveals shorter doubling time in big capsules: $PDT_{big} = 22\text{h} \pm 1\text{h}$
254 $< PDT_{small} = 25\text{h} \pm 1\text{h}$ (Fig. 5B).

255 Second, we pursued along our physiomimetic approach. Among all factors that make a stem cell niche, we have
256 already recapitulated interactions with the ECM. However, until now, we have omitted to consider oxygen
257 tension, which is known to be naturally low in developing embryos (43). This low level of oxygen was further
258 shown to be key to reduce mutation rates and epigenetic alterations (44, 45) as well as to improve the expansion
259 rate (46) while reducing the probability of unwanted differentiation (47). We thus performed the same culture
260 experiments in big capsules (300 μm radius) by decreasing the dissolved oxygen level (DO) from 100% to 20%.
261 (see Materials and Methods section). Under these hypoxic conditions, the population doubling time derived from
262 the growth kinetics was found to be $PDT_{big}^{hypoxia} = 20.4\text{h}$ (Fig. 5B), i.e, slightly but significantly shorter than in
263 normoxic conditions. Remarkably, this value is better than the one found at the single capsule level in normoxia,

264 suggesting that the optimization of capsule size and oxygen tension allowed to upscale the production of hPSCs in
265 a bench-scale bioreactor without any degradation of the expansion efficiency.

266 In order to assess whether this protocol is not only theoretically scalable but can be truly upscaled to an industrial
267 level, we carried out a final experiment in duplicate in a 10 L STBR (Fig. 5C, S8 and Movie S5) by keeping all
268 other parameters constant. Figure 5D shows the the expansion-fold as a function of time. The two curves from
269 these two independent experiments are superimposable and we found $AF_{10L\ STBR}(6.5\ days)=277$, corresponding to
270 a doubling time $PDT_{10L\ STBR}=19.6$ h.

271 These data were obtained without passaging. In order to assess the robustness of the approach for a seed train of
272 passaging and demonstrate that the technology can be integrated into a classical cell therapy production, we
273 performed serial passaging. At harvest after about 7 days, the capsules were dissolved, the 3D colonies were
274 dissociated and cells re-encapsulated following the same protocol (Fig. 6). We found that expansion-fold and
275 stemness were preserved over two consecutive encapsulations within 14 days (Fig. S9).

276

277 **DISCUSSION**

278 In this work, we have developed an *in vitro* culture system for hiPSCs, that we named C-STEM (Fig. 6) and
279 combines the benefits of biomimetic 3D culture and scalable bioreactor-based production. By contrast with other
280 approaches using scaffold embedding in bulk matrix (48) or hydrogel beads (49, 50), our hollow capsules allow
281 in-situ engineering of stem cell niche-like microenvironment. With biological and topological cues driving 3D
282 self-organization of hiPSCs colonies that are reminiscent of epiblasts (51). While cell-cell interactions are not
283 impaired due to the absence of enwrapping scaffold, the presence of the shell also provides mechanical protection
284 against impeller damage and turbulence-induced so-called Kolmogorov eddies during stirring (52). Besides
285 exploiting both the biomimetic and protective properties of the developed C-STEM platform, we have finally
286 refined the culture conditions by optimizing the initial mean number of cells per capsule and the oxygen tension.
287 Combination of all these critical factors allowed us to upscale the production of hPSCs and demonstrate that the

288 amplification efficiency is scale-independent. In particular, we could reach 282-fold amplification in 6.5 days in a
289 10 L stirred-tank bioreactor.

290 To the best of our knowledge, this level of both amplification and scalability is unmatched in the field (15, 53).

291 This technical and quantitative tour de force is actually related to the higher cell viability obtained in our hollow

292 capsules as compared with 2D cultures or other 3D suspension cultures. Since the amplification factor $AF(t)$ of a

293 culture system is given by $AF(t) = 2^{t/PDT}$, where PDT is the population doubling time and accounts both for cell

294 division and cell death, we may rewrite it as $AF(t) = 2^{(k_+ - k_-)t}$, where k_+ and k_- are respectively the division and

295 death rate of cells. Thus, the upper theoretical limit for AF is obtained for $k_-=0$ (i.e. infinite death time), which

296 then yields a minimal PDT_{min} value, equal to k_+ . Quite surprisingly, the measurement of k_+ or the duration of the

297 cell cycle $t_+=1/k_+$ of hiPSC has been overlooked in the literature. The sole report we are aware of arises from a

298 recent work in which cell cycle kinetics was tracked using a rainbow reporter in primed pluripotent stem cells

299 (54). The obtained cell cycle duration was found to be $t_+\sim 14$ h. While the question of “gemellarity” between

300 embryonic stem cells (ESC) and hiPSC is still under debate (55), this value is also consistent with previous

301 estimates of $t_+=11-16$ -h for the cell cycle duration in human and mammalian ESC (56–58). By assuming that the

302 duration of the cell cycle in the 3D cyst topology is identical to the value obtained in 2D cultures with $AF(t=6.5$

303 days)=282 corresponding to $PDT=19$ h, we find that the doubling time of the encapsulated hiPSC colonies is only

304 $5\text{h}\pm 2\text{h}$ longer than the intrinsic cell cycle duration. The difference corresponds to a death rate $k_-=1/53\text{h}^{-1}$. By

305 comparison, in the seminal Yamanaka’s paper (14), doubling times in 2D hiPSC colonies of about 45 h indicate

306 that $k_-=1/20\text{h}^{-1}$. More meaningful than the death rate k_- , the fraction of dead cells can be roughly estimated as

307 $\phi_{dead} \approx \frac{2^{k_-t}}{2^{PDT}} = 2.6\%$ at $t=6.5$ days, while cell counting gives 1.30% in bioreactors and 1.97% in flasks (Fig.S6). In

308 2D cultures, we measured a fraction of dead cells of the order of 12% at harvest, even though this value under-

309 estimates the cumulated mortality which is drastically impacted by cell passaging and confluency (59). Further

310 expansion improvement is theoretically within reach by vanishing the cell death rate. Taking again $t_+\sim 14$ h for the

311 cell cycle length of hiPSC, the glass ceiling is calculated to be $AF_{max}(t=6.5\text{ d})\sim 2200$. However, the value of $t_+\sim 14$

312 h cannot be taken as granted. For instance, a cell density-dependence on the proliferation rate has been reported.

313 Indeed, hPSC exhibit a decelerated proliferation due to a prolonged G1 phase as cell density increases (60).
314 Similarly, smaller expansion folds were observed when the inoculation density either as single cells or pre-
315 clusters in a synthetic hydrogel exceeds 10^6 cells/mL (48). We may then anticipate that the actual average cell
316 cycle duration could be longer than the one reported above upon single-cell lineage tracking in small colonies of
317 hPSCs. As a consequence, even though future work should aim at a rigorous *in situ* measurement of the division
318 rate within the encapsulated hiPSC cysts, we cannot exclude that the unprecedented hiPSC expansion rates
319 reported in this work are approaching the glass ceiling.

320 Among other specificities of the C-STEM technology, we mentioned the protective role of the alginate shell and
321 the scale-independence of the culture conditions. By contrast with other suspension cultures that need to design
322 specific low-shear impellers (e.g. the vertical-wheel bioreactor, (61, 62), or to add shear-dampener polymers (e.g.
323 pluronics, (24)) in order to avoid stirring-induced cell damages, our capsules permit the use of standard industrial
324 scale bioreactors.

325 However, all the benefits cannot be assigned to this sole shielding effect. Indeed, previous works had already
326 proposed to embed either hESC aggregates or microcarriers within hydrogel beads (which are referred to as
327 capsules in these original works) (50) to improve cell viability. Nonetheless, expansion rates were not reported to
328 be larger than 10 in 19 days. Similarly, two recent works describe stem cells encapsulation in hollow capsules (63,
329 64). However, the absence of ECM leads to the formation of aggregates and a modest amplification (estimated to
330 70-fold in 8 days from the size of the encapsulated spheroids). We thus propose that the significant amplification
331 increase obtained with the C-STEM technology mostly originates from the stem cell niche-like environment that
332 is engineered within each capsule and that drives hiPSC multicellular organization into cysts.

333 Interestingly, numerous studies have recently proposed biomimetic controllable environments that can be used to
334 develop hPSC-based embryo models and more specifically epiblast models (22, 65, 66). In all cases, these 3D
335 stem cell niche mimics drive PSCs self-organization, luminogenesis, and polarization into pseudo-stratified
336 epithelia (19–21). This cyst configuration, which seems to be key in developmental processes, may be regarded as
337 an optimized configuration for hPSC expansion with minimal loss of viability (67). First, it is well accepted that

338 2D hiPSC cultures exhibit intra-colony heterogeneities in pluripotency marker genes (68), viability (69) and cell
339 morphology (70), which are very striking between the center and the edges of the colonies. In this respect, the
340 closed spherical symmetry of a cyst intrinsically suppresses the “center-edge phenotype” and may result in more
341 homogeneous cell population (71). Additionally, whereas cellular crowding or compaction are known to inhibit
342 proliferation or even trigger apoptosis via caspase-dependent mechanisms (72) a cyst configuration is less prone
343 to stress building in bulk due to the presence of a lumen. Similarly, fast proliferation rate may contribute to stress
344 relaxation and reduce cell extrusion occurrence as observed in epithelia under compression (73, 74). Besides
345 mechanical stress, chemical stresses are known to increase the mutation rate (44, 75). The use of bioreactors with
346 precise adjustment of physioxia, pH, lactate, glucose and nutriments supply is thus instrumental and could be
347 optimized beyond the present achievement.

348 Finally, relying on the observation that chromosome segregation fidelity is unambiguously higher in native
349 contexts of epithelia of primary cells (76, 77), it also becomes tempting to speculate that, beyond the gain in
350 amplification it provides, the preserved histology of our *in-vitro* epiblast-like colonies could also be beneficial to
351 the maintenance of the genetic integrity (78).

352

353 In summary, our work has shown that hollow alginate capsules with reconstituted niche-like microenvironment
354 can promote the formation and growth of 3D hPSC colonies and provide the necessary protection for scaling up
355 the production in stirred tank bioreactors. Self-organized encapsulated epiblast-like colonies seem to be
356 instrumental for optimal expansion by preserving stem cells physiological properties. We have demonstrated that
357 our biomimetic stem cell platform C-STEM can deliver unprecedented scalability and we anticipate that cell
358 quality is preserved on the basis of extremely high viability, which is taken as a primary signature of cell fitness.
359 Future works should focus on assessing the hPSCs quality in *in vivo*-like culture systems, since the emergence of
360 mutations during culture may be the last limitation to overcome for cell therapy bioproduction.

361 **MATERIALS AND METHODS**

362 *Ethics statements*

363 The generation, use and storage of hiPSCs were performed with approval from the “Comité de Protection des
364 Personnes” (CPP) Ile de France (DC 2015-2595 and 2016-A00773-48).

365 *Human pluripotent stem cell lines*

366 Throughout the present work, we used 4 hiPSC lines. Among these, 3 hiPS cells, namely IMAGINi004-A
367 (referred to as iPS004), IMAGINi005-A (iPS005) and IMAGINi013-A (iPS013) were derived from peripheral
368 blood mononuclear cells (PBMC) according to the protocol described in (34). Briefly, PBMCs were transduced
369 using the CytoTune-iPS 2.0 Sendai Reprogramming Kit (ThermoFisher Scientific) following the manufacturer's
370 instructions. After 2-3 weeks, colonies were manually picked and expanded at least 10 passages. The 4th hiPSC
371 line is a commercial line from ThermoFisher: Gibco™ episomal hiPSC line (A18945) generated using cord blood
372 derived CD34+ progenitors with 7 episomally expressed factors (Oct4, Sox2, Klf4, Myc, Nanog, Lin28, and
373 SV40 T). This commercial cell line is referred to as iPS C. For the sake of availability, in order to allow other
374 groups to reproduce our findings, all experiments reported here were performed with iPS C, except for those that
375 are described in Figures 2F, 3A,B,D 4E and Figures S4 S5, which were carried out to demonstrate that the
376 findings were not cell line-dependent.

377 *2D hiPSC culture*

378 All hiPSC lines were maintained on Matrigel (Corning Ref. 354234) and cultured in mTeSR1 medium (StemCell
379 Technologies 85875). Cultures were fed daily, passaged with an enzyme-free reagent, ReleSR (StemCell
380 Technologies 05873) every 3-6 days (around 80% confluency) and replated as small clusters (between 100 and
381 200 μm) at a density of about 5000-10000 cells/cm². Cells were cultured at 37°C in a humidified atmosphere
382 containing 5% CO₂.

383 *3D hiPSC Encapsulation*

384 Prior to encapsulation, 2D stem cell colonies were detached using ReLeSR for 1 minute and dissociated into a
385 near single cell solution using Accutase (Stem Cell Technologies 07920). HiPSCs were then mixed in a 50/50

386 volume ratio with Matrigel at 4°C to keep the suspension in a liquid state. The final concentration of cells in the
387 cell/matrix solution was thus between 0.4-1.0×10⁶ viable cells/mL, referred to as the encapsulation density. The
388 encapsulation system is similar to the one described in (29). In brief, ethylene tetrafluoroethylene (ETFE,) tubings
389 are connected to the three inlets of a 3D printed (using the DLP Micro Plus Hi-Res printer from EnvisionTEC)
390 microfluidic co-laminar flow device. An extruded and polished glass microcapillary tip (of diameter ~100 μm for
391 most experiments reported in this work, at the exception of those shown in Fig. 5A-B that were carried out with a
392 nozzle diameter of 150 μm) is glued to the outlet of the nozzle for a better control of the flow. The cell/matrix
393 suspension is loaded into the inner channel of the 3-way device, which is kept refrigerated thanks to an in-line
394 cooling system in order to prevent premature gelation of Matrigel. A solution of sodium alginate (Novamatrix
395 Pronova SLG100, 0,25 g #4202101 at 2% in distilled water) is injected into the outer channel. To prevent alginate
396 gelation within the microfluidic device due to calcium release from the suspended cells, a calcium-free solution
397 (Sorbitol 300mM, Sigma-Aldrich 85529) is used in the intermediate channel of the co-extrusion chip and serves
398 as a barrier against calcium diffusion. Typical flow rates for the 3 solutions were on the order of 120 ml/h for all
399 three channels: (alginate solution, the sorbitol solution and the cell+matrix suspension). At these rates, the
400 composite solution forms a liquid jet that fragments into droplets (of about twice the size of the nozzle) due to the
401 spontaneous Rayleigh-Plateau instability. To avoid subsequent coalescence of the train of droplet, an alginate
402 charging part and a copper ring are connected to a high voltage (2000V) generator are introduced. A high-speed
403 camera (PHANTOM VEO 1310L) was used to visualize droplet formation and splay (Fig. S1 and Movie S1).
404 When the composite droplets contact the collecting calcium bath (at 100mM), the outer layer of alginate readily
405 gels. As a consequence, the inner cell/matrix solution remains entrapped inside a closed, spherical and
406 permeable micro-compartment. Within 1 min following encapsulation, capsules are rinsed with medium (DMEM)
407 to reduce the basal calcium concentration. Finally, they are transferred to suspension culture medium.

408 Re-encapsulation was performed by dissolution of alginate shells using short rReleSR rinse, followed by cell
409 dissociation using TrypLE (Trypsin-based, dissociation enzyme, ThermoFischer) for 20 minutes at 37°. Then the
410 obtained cells were processed following the classic encapsulation protocol.

411 ***3D stem cell suspension culture in static T-Flasks or bioreactors***

412 Static suspension cultures of encapsulated hiPSC were carried out using T-Flasks (from 5 to 30 ml) maintained in
413 a cell culture incubator at 37°C and 5% CO₂. The medium (mTeSR1) was supplemented with 10μM Y-27632 for
414 ROCK inhibition only during the first 24 hours of culture. From culture day 3, the medium was exchanged every
415 day as described hereafter. The contents of the T-Flasks were transferred into Falcon Tubes. After capsules
416 sedimentation (within a few minutes), the supernatant was removed and replenished as the capsules were
417 transferred back into a T-Flasks. The volume of culture medium was kept constant for the first 4 days of culture
418 (~ 4× the capsules volume). Then, the volume was steadily increased every day in order to maintain a cell
419 concentration below 10⁶ cells/mL.

420 Stirred suspension cultures were performed in different bioreactors. For all experiments reported in Fig. 4 and Fig.
421 5A-B, we used benchtop STBRs, including a 30 mL (Minibio, ABLE® Bioreactor Systems) or 500 mL
422 bioreactors (Applikon Biotechnology & Global Process Concept). For the experiments reported in Fig. 5C-D, we
423 used a 10 liter -scale bioreactor (Global Process Concept).

424 In all cases, the bioreactors were inoculated with 15% capsule-to-medium volume. The bioreactor culture starts at
425 a volume representing 30% of the final working volume. At Day1, the medium was replaced with fresh medium
426 without ROCK inhibitor. From day 2 to 5, the culture is performed in a fed-batch mode up to the final working
427 volume (39). Then, we switched to repeated-batch mode, where 90% of the media was daily renewed to maintain
428 sufficient nutrient supply. The final capsule-to-medium volume was $4.2 \pm 0.3\%$ and the pH was maintained at
429 7.2 ± 0.2 .

430 Dissolved Oxygen (DO) level is calibrated at 100% in starting conditions by injecting air into the bioreactor
431 headspace. During the run, the oxygen level is monitored and controlled. In normoxic conditions the oxygen is
432 controlled at 100% while in hypoxic conditions the set point is at 20% DO. Oxygen level is regulated by sparging
433 nitrogen and/or air to maintain the set point. 10L scale bioreactors were regulated in hypoxic conditions. During
434 one week of culture, the stirring speed is set at 150 rpm that is sufficient to keep capsules resuspension and
435 bioreactor homogeneity along the run.

436 ***Time-lapse microscopy of encapsulated cyst growth and image analysis***

437 Time-lapse microscopy was performed using a Nikon Biostation IM microscope with a 10x objective. Capsules
438 containing hiPSCs were transferred to a 35 mm Petri dish 24 hours after encapsulation. Approximately 10 to 20
439 capsules were placed in the petri dish containing 5 mL of fresh Y-27632-free mTeSR1 medium. Cyst growth was
440 monitored over 7 days. Practically, images were taken every 6 to 10 minutes at preselected Z-focal planes to
441 ensure acquisition at proper focus in case of undesired drift Image analysis was performed using ImageJ. The
442 external and internal effective radii of the cysts, R_{out} and R_{in} , were measured from the equatorial corresponding
443 cross sections S according to $R_{out,in}=(S_{out,in}/\pi)^{1/2}$ after applying appropriate bandpass filters and thresholds. The
444 volume V of the cells was calculated as $V=4\pi/3(R_{out}^3-R_{in}^3)$. Capsule circularity was defined as $C=a^2/b^2$, where a
445 and b are the short and long axes of the approximated ellipse.

446 ***In vitro trilineage differentiation***

447 Small cell clusters were collected from hiPSC cultures (2D or decapsulated-dissociated 3D hiPSCs colonies) and
448 transferred into low attachment dishes (Corning, Ultra-low attachment 6 well plate). Three-dimensional
449 aggregates of cells that are an amalgam of the three developmental germ layers (Embryoid bodies) are obtained
450 and cultured in suspension for 7 to 9 days with DMEM/F-12 medium containing 20% pluriQ Serum Replacement
451 (GlobalStem), 1% non-essential amino acids, 1% penicillin-streptomycin and 0.2% β -mercaptoethanol
452 (ThermoFisher Scientific) in a humidified atmosphere containing 5% CO₂. Culture medium was refreshed every
453 two days. EBs were then collected for RNA analyses or transferred onto gelatin-coated dishes for 1 week. For
454 immunocytochemistry analysis, cells were fixed with 4% paraformaldehyde for 15 min at room temperature (RT).
455 After washing in PBS/1%BSA blocking solution for 1 hour, cells were incubated overnight at 4°C with primary
456 antibodies, washed 3 times in PBS, and incubated with secondary antibodies for 2 hours at RT. Antibodies were
457 diluted in PBS/1%BSA/0.1%triton solution. The list of antibodies used in this work and their origin are listed in
458 Table S1. Nuclei were stained with a DAPI solution. Immuno-fluorescence staining was analyzed using the
459 Celena S™ Digital Imaging System (Logos Biosystems).

460 ***RNA extraction and RT-PCR analyses***

461 Total RNA was extracted using the RNeasy Mini Kit (Qiagen). cDNA was synthesized using a high capacity
462 cDNA RT kit (ThermoFisher Scientific) from 1 μ g of total RNA. The expression of pluripotency markers as well

463 as the trilineage differentiation potential of the cells were evaluated by TaqMan® hiPSC Scorecard™ assay
464 according to the manufacturer's protocol. This scorecard compares the gene expression pattern of key
465 pluripotency and germ lineage markers relative to a reference standard that consists of 9 different human ES and
466 iPS lines. Data analysis was performed using the cloud based TaqMan® hiPSC Scorecard™ analysis software.

467 ***DNA isolation, genomic stability and authenticity analysis***

468 DNA isolation was performed using the PureLink™ Genomic DNA Mini Kit (Invitrogen). Molecular karyotype
469 was performed using an Infinium Core-24 v1.2 Kit (Illumina) containing 300000 SNPs. Data were analyzed with
470 BeadStudio/GenomeStudio software (Illumina). The percentage of SNP concordance between iPSC samples
471 before and 7 days after encapsulation was assessed for the 3 derived iPSC cell lines. SNP files of all samples were
472 extracted from genome studio software. The percentage of concordance between two paired samples (before and
473 after encapsulation) was evaluated by comparing the genotype of each informative SNP (Fig. S5)

474 ***Flow cytometry analysis***

475 The hiPSCs colonies were dissociated with Accutase for 10 minutes at 37°C for 2D cultures or with TrypLE
476 Select (ThermoFisher Scientific 11598846) for 30 minutes at 37°C for 3D cultures after capsule removal. Then,
477 cells were fixed and permeabilized using the Transcription Factor Staining Buffer Set (ThermoFisher 11500597).
478 Cells were suspended in the permeabilization buffer at a density of $0.5-1 \times 10^6$ cells in 100 µl and incubated with
479 the specific antibodies or isotype controls (Table S1) for 45 minutes at room temperature in the dark. Cells were
480 washed twice with the staining buffer and analyzed using either BD Canto II (at the TBMCORE CNRS UMS 3427
481 – INSERM US 005) or a BD Accuri™ C6 plus and data was post-processed with FlowJo software.

482 ***Cell growth and viability analysis***

483 Cell counting was performed using the Nucleo counter NC3000 or NC200 (Chemometec). Live/dead analysis was
484 performed using CalceinAM/Ethidium homodimer-1 (ThermoFisher L3224) according to the manufacturer
485 recommendations, and samples were imaged using either the EVOS FL or EVOS M5000 auto Imaging system
486 (ThermoFischer).

487 ***Immunostaining, Microscopy, and Image Analysis***

488 For daily brightfield imaging of 2D cultures and encapsulated hiPSC cysts, a widefield EVOS FL or EVOS
489 M5000 automated microscope was used. Encapsulated 3D hiPSC colonies were harvested for confocal
490 microscopy at several timepoints. The alginate capsule was removed prior to fixation by incubating the samples in
491 PBS without divalent cations for at least 5 minutes with agitation at RT. Both 2D and 3D stem cell colonies were
492 fixed with 4% PFA for 30-60 minutes at RT in the dark. Following fixation, the samples were washed 3x with
493 0.1% Tween20 in PBS. A permeabilization step was done in parallel with excess PFA quenching in a PBS
494 solution containing 0.3% Triton X-100 and 100 mM Glycine for 30 minutes, followed by 3x washing with 0.1%
495 Tween20 in PBS. The samples were incubated in primary and secondary antibodies (Table S1) in 1% BSA +
496 0.1% Tween20 in PBS overnight at 4° with gentle orbital agitation, including a 3x rinsing with 1% BSA + 0.1%
497 Tween20 in PBS after each incubation. To maintain alginate capsules during fixation and staining, the
498 decapsulation step was skipped and all solutions (including 4% PFA) were supplemented with calcium and
499 magnesium. All samples were imaged on either a Leica SP5 or SP8 confocal microscope (Bordeaux Imaging
500 Center, BIC).

501 *Statistical Analysis*

502 All statistical analyses were performed using GraphPad Prism8. To test significant differences between bioreactor
503 and flask, 2wayANOVA with sidak's multiple comparison test was used. To compare between 2 groups, a
504 student T-test was used. All statistical significance is reported in terms of p-values <0.05.

505 **REFERENCES**

506

- 507 1. O. Lindvall, S. Rehn, P. Brundin, B. Gustavii, B. Åstedt, H. Widner, T. Lindholm, A. Bjorklund, K.
508 L. Leenders, J. C. Rothwell, R. Frackowiak, C. D. Marsden, B. Johnels, G. Steg, R. Freedman, B. J.
509 Hoffer, A. Seiger, M. Bygdeman, I. Strömberg, L. Olson, Human fetal dopamine neurons grafted into the
510 striatum in two patients with severe parkinson's disease: A detailed account of methodology and a 6-
511 month follow-up. *Archives of Neurology*. **46**, 615–631 (1989).
- 512 2. M. Parmar, S. Grealish, C. Henchcliffe, The future of stem cell therapies for Parkinson disease. *Nature*
513 *Reviews Neuroscience*. **21**, 103–115 (2020).
- 514 3. Shapiro, Islet transplantation in seven patients with type 1 diabetes mellitus using a glucocorticoid-free
515 immunosuppressive regimen. *NEJM* (2000).
- 516 4. J. B. Sneddon, Q. Tang, P. Stock, J. A. Bluestone, S. Roy, T. Desai, M. Hebrok, Stem Cell Therapies for
517 Treating Diabetes: Progress and Remaining Challenges. *Cell Stem Cell*. **22**, 810–823 (2018).
- 518 5. M. Mandai, A. Watanabe, Y. Kurimoto, Y. Hirami, C. Morinaga, T. Daimon, M. Fujihara, H. Akimaru, N.
519 Sakai, Y. Shibata, M. Terada, Y. Nomiya, S. Tanishima, M. Nakamura, H. Kamao, S. Sugita, A. Onishi, T.
520 Ito, K. Fujita, S. Kawamata, M. J. Go, C. Shinohara, K. Hata, M. Sawada, M. Yamamoto, S. Ohta, Y.
521 Ohara, K. Yoshida, J. Kuwahara, Y. Kitano, N. Amano, M. Umekage, F. Kitaoka, A. Tanaka, C. Okada,
522 N. Takasu, S. Ogawa, S. Yamanaka, M. Takahashi, Autologous Induced Stem-Cell-Derived Retinal Cells
523 for Macular Degeneration. *New England Journal of Medicine*. **376**, 1038–1046 (2017).
- 524 6. P. Menasché, A. A. Hagege, M. Scorsin, B. Pouzet, M. Desnos, D. Duboc, K. Schwartz, J. T. Vilquin, J. P.
525 Marolleau, Myoblast transplantation for heart failure. *Lancet*. **357**, 279–280 (2001).
- 526 7. C. E. Murry, W. R. MacLellan, Stem cells and the heart - The road ahead. *Science*. **367**, 854–855 (2020).
- 527 8. J. Deinsberger, D. Reisinger, B. Weber, Global trends in clinical trials involving pluripotent stem cells: a
528 systematic multi-database analysis. *npj Regenerative Medicine*. **5**, 1–13 (2020).
- 529 9. J. X. Yu, S. Upadhaya, R. Tataka, F. Barkalow, V. M. Hubbard-Lucey, Cancer cell therapies: the clinical
530 trial landscape. *Nature reviews. Drug discovery*. **19**, 583–584 (2020).

- 531 10. R. Sender, S. Fuchs, R. Milo, Revised Estimates for the Number of Human and Bacteria Cells in the Body.
532 *PLoS Biology*. **14**, 1–14 (2016).
- 533 11. M. J. Evans, M. H. Kaufman, Establishment in culture of pluripotential cells from mouse embryos. *Nature*.
534 **292** (1981), pp. 154–156.
- 535 12. G. R. Martin, Isolation of a pluripotent cell line from early mouse embryos cultured in medium
536 conditioned by teratocarcinoma stem cells. *Proceedings of the National Academy of Sciences of the United*
537 *States of America*. **78**, 7634–7638 (1981).
- 538 13. J. A. Thomson, Embryonic stem cell lines derived from human blastocysts. *Science*. **282**, 1145–1147
539 (1998).
- 540 14. K. Takahashi, K. Tanabe, M. Ohnuki, M. Narita, T. Ichisaka, K. Tomoda, S. Yamanaka, Induction of
541 Pluripotent Stem Cells from Adult Human Fibroblasts by Defined Factors. *Cell*. **131**, 861–872 (2007).
- 542 15. M. M. Adil, D. v. Schaffer, Expansion of human pluripotent stem cells. *Current Opinion in Chemical*
543 *Engineering*. **15**, 24–35 (2017).
- 544 16. E. Kuijk, M. Jager, B. van der Roest, M. Locati, A. van Hoeck, J. Korzelius, R. Janssen, N. Besselink, S.
545 Boymans, R. van Boxtel, E. Cuppen, Mutational impact of culturing human pluripotent and adult stem
546 cells. *Nature Communications*, 430165 (2018).
- 547 17. K. Garber, RIKEN suspends first clinical trial involving induced pluripotent stem cells. *Nature*
548 *biotechnology*. **33**, 890–891 (2015).
- 549 18. S. Yamanaka, Pluripotent Stem Cell-Based Cell Therapy-Promise and Challenges. *Cell stem cell*. **27**, 523–
550 531 (2020).
- 551 19. K. Taniguchi, Y. Shao, R. F. Townshend, Y. H. Tsai, C. J. DeLong, S. A. Lopez, S. Gayen, A. M. Freddo,
552 D. J. Chue, D. J. Thomas, J. R. Spence, B. Margolis, S. Kalantry, J. Fu, K. S. O’Shea, D. L. Gumucio,
553 Lumen Formation Is an Intrinsic Property of Isolated Human Pluripotent Stem Cells. *Stem Cell Reports*. **5**,
554 954–962 (2015).
- 555 20. M. N. Shahbazi, A. Scialdone, N. Skorupska, A. Weberling, G. Recher, M. Zhu, A. Jedrusik, L. G. Devito,
556 L. Noli, I. C. MacAulay, C. Buecker, Y. Khalaf, D. Ilic, T. Voet, J. C. Marioni, M. Zernicka-Goetz,

- 557 Pluripotent state transitions coordinate morphogenesis in mouse and human embryos. *Nature*. **552**, 239–
558 243 (2017).
- 559 21. Y. Zheng, X. Xue, Y. Shao, S. Wang, S. N. Esfahani, Z. Li, J. M. Muncie, J. N. Lakins, V. M. Weaver, D.
560 L. Gumucio, J. Fu, Controlled modelling of human epiblast and amnion development using stem cells.
561 *Nature*. **573**, 421–425 (2019).
- 562 22. M. N. Shahbazi, Mechanisms of human embryo development: from cell fate to tissue shape and back.
563 *Development (Cambridge)*. **147** (2020).
- 564 23. M. A. Kinney, C. Y. Sargent, T. C. McDevitt, The multiparametric effects of hydrodynamic environments
565 on stem cell culture. *Tissue Engineering - Part B: Reviews*. **17**, 249–262 (2011).
- 566 24. F. Manstein, K. Ullmann, C. Kropp, C. Halloin, W. Triebert, A. Franke, C. M. Farr, A. Sahabian, A.
567 Haase, Y. Breitzkreuz, M. Peitz, O. Brüstle, S. Kalies, U. Martin, R. Olmer, R. Zweigerdt, High density
568 bioprocessing of human pluripotent stem cells by metabolic control and in silico modeling. *Stem Cells*
569 *Translational Medicine*, 1–18 (2021).
- 570 25. B. S. Borys, T. So, J. Colter, T. Dang, E. L. Roberts, T. Revay, L. Larijani, R. Krawetz, I. Lewis, B.
571 Argiropoulos, D. E. Rancourt, S. Jung, Y. Hashimura, B. Lee, M. S. Kallos, Optimized serial expansion of
572 human induced pluripotent stem cells using low-density inoculation to generate clinically relevant
573 quantities in vertical-wheel bioreactors. *Stem Cells Translational Medicine*. **9**, 1036–1052 (2020).
- 574 26. M. Ma, A. Chiu, G. Sahay, J. C. Doloff, N. Dholakia, R. Thakrar, J. Cohen, A. Vegas, D. Chen, K. M.
575 Bratlie, T. Dang, R. L. York, J. Hollister-Lock, G. C. Weir, D. G. Anderson, Core-Shell Hydrogel
576 Microcapsules for Improved Islets Encapsulation. *Advanced Healthcare Materials*. **2**, 667–672 (2013).
- 577 27. W. Zhang, S. Zhao, W. Rao, J. Snyder, J. K. Choi, J. Wang, I. A. Khan, N. B. Saleh, P. J. Mohler, J. Yu,
578 T. J. Hund, C. Tang, X. He, A novel core-shell microcapsule for encapsulation and 3D culture of
579 embryonic stem cells. *Journal of Materials Chemistry B*. **1**, 1002–1009 (2013).
- 580 28. K. Alessandri, B. R. Sarangi, V. V. Gurchenkov, B. Sinha, T. R. Kießling, L. Fetler, F. Rico, S. Scheuring,
581 C. Lamaze, A. Simon, S. Geraldo, D. Vignjević, H. Doméjean, L. Rolland, A. Funfak, J. Bibette, N.
582 Bremond, P. Nassoy, Cellular capsules as a tool for multicellular spheroid production and for investigating

- 583 the mechanics of tumor progression in vitro. *Proceedings of the National Academy of Sciences of the*
584 *United States of America*. **110**, 14843–14848 (2013).
- 585 29. K. Alessandri, M. Feyeux, B. Gurchenkov, C. Delgado, A. Trushko, K.-H. H. Krause, D. Vignjević, P.
586 Nassoy, A. A. Roux, D. Vignjevic, P. Nassoy, A. A. Roux, A 3D printed microfluidic device for
587 production of functionalized hydrogel microcapsules for culture and differentiation of human Neuronal
588 Stem Cells (hNSC). *Lab Chip*. **16**, 1593–1604 (2016).
- 589 30. S. Tomotika, On the instability of a cylindrical thread of a viscous liquid surrounded by another viscous
590 fluid. *Proceedings of the Royal Society of London. Series A - Mathematical and Physical Sciences*. **150**,
591 322–337 (1935).
- 592 31. J. P. Freyei, R. M. Sutherland, Regulation of Growth Saturation and Development of Necrosis in EMT6/R0
593 Multicellular Spheroids by the Glucose and Oxygen Supply. *Cancer Research*. **46**, 3504–3512 (1986).
- 594 32. B. S. Freedman, C. R. Brooks, A. Q. Lam, H. Fu, R. Morizane, V. Agrawal, A. F. Saad, M. K. Li, M. R.
595 Hughes, R. vander Werff, D. T. Peters, J. Lu, A. Baccei, A. M. Siedlecki, M. T. Valerius, K. Musunuru, K.
596 M. McNagny, T. I. Steinman, J. Zhou, P. H. Lerou, J. v. Bonventre, Modelling kidney disease with
597 CRISPR-mutant kidney organoids derived from human pluripotent epiblast spheroids. *Nature*
598 *Communications*. **6:8715** (2015).
- 599 33. S. D. Sheridan, V. Surampudi, R. R. Rao, Analysis of embryoid bodies derived from human induced
600 pluripotent stem cells as a means to assess pluripotency. *Stem Cells International*. **2012** (2012).
- 601 34. E. Quelennec, C. Banal, M. Hamlin, D. Clémantine, M. Michael, N. Lefort, E. Quelennec, C. Banal, M.
602 Hamlin, D. Clémantine, M. Michael, N. Lefort, Generation of two induced pluripotent stem cell lines
603 IMAGINi004-A and IMAGINi005-A from healthy donors. *Stem Cell Research*, 101959 (2020).
- 604 35. A. M. Tsankov, V. Akopian, R. Pop, S. Chetty, C. A. Gifford, L. Daheron, N. M. Tsankova, A. Meissner,
605 A qPCR ScoreCard quantifies the differentiation potential of human pluripotent stem cells. *Nature*
606 *Biotechnology*. **33**, 1182–1192 (2015).

- 607 36. C. Bock, E. Kiskinis, G. Verstappen, H. Gu, G. Boulting, Z. D. Smith, M. Ziller, G. F. Croft, M. W.
608 Amoroso, D. H. Oakley, A. Gnirke, K. Eggan, A. Meissner, Reference maps of human es and ips cell
609 variation enable high-throughput characterization of pluripotent cell lines. *Cell*. **144**, 439–452 (2011).
- 610 37. S. Assou, J. Bouckenheimer, J. de Vos, Concise Review: Assessing the Genome Integrity of Human
611 Induced Pluripotent Stem Cells: What Quality Control Metrics? *Stem Cells*. **36**, 814–821 (2018).
- 612 38. T. E. Ludwig, M. E. Levenstein, J. M. Jones, W. T. Berggren, E. R. Mitchen, J. L. Frane, L. J. Crandall, C.
613 A. Daigh, K. R. Conard, M. S. Piekarczyk, R. A. Llanas, J. A. Thomson, Derivation of human embryonic
614 stem cells in defined conditions. *Nature Biotechnology*. **24**, 185–187 (2006).
- 615 39. C. Kropp, D. Massai, R. Zweigerdt, Progress and challenges in large-scale expansion of human pluripotent
616 stem cells. *Process Biochemistry*. **59**, 244–254 (2017).
- 617 40. M. S. Croughan, J. P. Hamel, D. I. C. Wang, Effects of microcarrier concentration in animal cell culture.
618 *Biotechnology and Bioengineering*. **32**, 975–982 (1988).
- 619 41. C. J. Hewitt, K. Lee, A. W. Nienow, R. J. Thomas, M. Smith, C. R. Thomas, Expansion of human
620 mesenchymal stem cells on microcarriers. *Biotechnology Letters*. **33**, 2325–2335 (2011).
- 621 42. D. E. Kehoe, D. Jing, L. T. Lock, E. S. Tzanakakis, D. Ph, Scalable Stirred-Suspension Bioreactor Culture.
622 *Tissue Engineering: Part A*. **16**, 405–421 (2010).
- 623 43. M. C. Simon, B. Keith, The role of oxygen availability in embryonic development and stem cell function.
624 *Nature Reviews Molecular Cell Biology*. **9**, 285–296 (2008).
- 625 44. O. Thompson, F. von Meyenn, Z. Hewitt, J. Alexander, A. Wood, R. Weightman, S. Gregory, F. Krueger,
626 S. Andrews, I. Barbaric, P. J. Gokhale, H. D. Moore, W. Reik, M. Milo, S. Nik-Zainal, K. Yusa, P. W.
627 Andrews, Low rates of mutation in clinical grade human pluripotent stem cells under different culture
628 conditions. *Nature Communications*. **11**, 1528 (2020).
- 629 45. K. Okazaki, E. Maltepe, Oxygen, epigenetics and stem cell fate. *Regenerative medicine*. **1**, 71–83 (2006).
- 630 46. B. Abecasis, T. Aguiar, É. Arnault, R. Costa, P. Gomes-Alves, A. Aspegren, M. Serra, P. M. Alves,
631 Expansion of 3D human induced pluripotent stem cell aggregates in bioreactors: Bioprocess intensification
632 and scaling-up approaches. *Journal of Biotechnology*. **246**, 81–93 (2017).

- 633 47. T. Ezashi, P. Das, R. M. Roberts, Low O₂ tensions and the prevention of differentiation of HES cells.
634 *Nature Methods*. **2**, 325 (2005).
- 635 48. Y. Lei, D. v. Schaffer, A fully defined and scalable 3D culture system for human pluripotent stem cell
636 expansion and differentiation. *Proceedings of the National Academy of Sciences of the United States of*
637 *America*. **110**, E5039–E5048 (2013).
- 638 49. S. Swioklo, P. Ding, A. W. Patek, C. J. Connon, Process parameters for the high-scale production of
639 alginate-encapsulated stem cells for storage and distribution throughout the cell therapy supply chain.
640 *Process Biochemistry*. **59**, 289–296 (2017).
- 641 50. M. Serra, C. Correia, R. Malpique, C. Brito, J. Jensen, P. Bjorquist, M. J. T. Carrondo, P. M. Alves, M.
642 Serra, C. Correia, R. Malpique, C. Brito, J. Jensen, P. Bjorquist, M. J. T. Carrondo, P. M. Alves,
643 Microencapsulation technology: A powerful tool for integrating expansion and cryopreservation of human
644 embryonic stem cells. *PLoS ONE*. **6**, 1–13 (2011).
- 645 51. M. N. Shahbazi, M. Zernicka-Goetz, Deconstructing and reconstructing the mouse and human early
646 embryo. *Nature Cell Biology*. **20**, 878–887 (2018).
- 647 52. K. Ponnuru, J. Wu, P. Ashok, E. S. Tzanakakis, E. P. Furlani, Analysis of stem cell culture performance in
648 a microcarrier bioreactor system. *Technical Proceedings of the 2014 NSTI Nanotechnology Conference*
649 *and Expo, NSTI-Nanotech 2014*. **2**, 132–135 (2014).
- 650 53. A. Polanco, B. Kuang, S. Yoon, Bioprocess Technologies that Preserve the Quality of iPSCs. *Trends in*
651 *Biotechnology*. **xx**, 1–13 (2020).
- 652 54. D. El-Nachef, K. Shi, K. M. Beussman, R. Martinez, M. C. Regier, G. W. Everett, C. E. Murry, K. R.
653 Stevens, J. E. Young, N. J. Sniadecki, J. Davis, A Rainbow Reporter Tracks Single Cells and Reveals
654 Heterogeneous Cellular Dynamics among Pluripotent Stem Cells and Their Differentiated Derivatives.
655 *Stem Cell Reports*. **15**, 226–241 (2020).
- 656 55. K. H. Narsinh, J. Plews, J. C. Wu, Comparison of human induced pluripotent and embryonic stem cells:
657 Fraternal or identical twins? *Molecular Therapy*. **19**, 635–638 (2011).

- 658 56. L. Liu, W. Michowski, A. Kolodziejczyk, P. Sicinski, The cell cycle in stem cell proliferation,
659 pluripotency and differentiation. *Nature Cell Biology*. **21**, 1060–1067 (2019).
- 660 57. K. W. Orford, D. T. Scadden, Deconstructing stem cell self-renewal: Genetic insights into cell-cycle
661 regulation. *Nature Reviews Genetics*. **9**, 115–128 (2008).
- 662 58. J. Padgett, S. D. Santos, From clocks to dominoes: lessons on cell cycle remodelling from embryonic stem
663 cells. *FEBS Letters*. **594**, 2031–2045 (2020).
- 664 59. Q. Li, H. Lin, Q. Du, K. Liu, O. Wang, C. Evans, H. Christian, C. Zhang, Y. Lei, Scalable and
665 physiologically relevant microenvironments for human pluripotent stem cell expansion and differentiation.
666 *Biofabrication*. **10** (2018).
- 667 60. J. Wu, Y. Fan, E. S. Tzanakakis, Increased Culture Density Is Linked to Decelerated Proliferation,
668 Prolonged G1 Phase, and Enhanced Propensity for Differentiation of Self-Renewing Human Pluripotent
669 Stem Cells. *Stem Cells and Development*. **24**, 892–903 (2015).
- 670 61. B. S. Borys, T. Dang, T. So, L. Rohani, T. Revay, T. Walsh, M. Thompson, B. Argiropoulos, D. E.
671 Rancourt, S. Jung, Y. Hashimura, B. Lee, M. S. Kallos, Overcoming bioprocess bottlenecks in the large-
672 scale expansion of high-quality hiPSC aggregates in vertical-wheel stirred suspension bioreactors. *Stem*
673 *Cell Research and Therapy*. **12**, 1–19 (2021).
- 674 62. D. E. S. Nogueira, C. A. V. Rodrigues, M. S. Carvalho, C. C. Miranda, Y. Hashimura, S. Jung, B. Lee, J.
675 M. S. Cabral, Strategies for the expansion of human induced pluripotent stem cells as aggregates in single-
676 use Vertical-WheelTM bioreactors. *Journal of Biological Engineering*. **13**, 1–14 (2019).
- 677 63. P. Fattahi, A. Rahimian, M. Q. Slama, K. Gwon, A. M. Gonzalez-Suarez, J. Wolf, H. Baskaran, C. D.
678 Duffy, G. Stybayeva, Q. P. Peterson, A. Revzin, Core–shell hydrogel microcapsules enable formation of
679 human pluripotent stem cell spheroids and their cultivation in a stirred bioreactor. *Scientific Reports*. **11**,
680 1–13 (2021).
- 681 64. I. Horiguchi, Y. Sakai, Alginate Encapsulation of Pluripotent Stem Cells Using a Co-axial Nozzle. *Journal*
682 *of Visualized Experiments*, 1–7 (2015).

- 683 65. S. Vianello, M. P. Lutolf, Understanding the Mechanobiology of Early Mammalian Development through
684 Bioengineered Models. *Developmental Cell*. **48**, 751–763 (2019).
- 685 66. A. M. Resto Irizarry, S. Nasr Esfahani, J. Fu, Bioengineered pluripotent stem cell models: new approaches
686 to explore early human embryo development. *Current Opinion in Biotechnology*. **66**, 52–58 (2020).
- 687 67. Y. Zhu, H. Wang, F. Yin, Y. Guo, F. Li, D. Gao, J. Qin, Amnion-on-a-chip: modeling human amniotic
688 development in mid-gestation from pluripotent stem cells. *Lab on a Chip*. **20**, 3258–3268 (2020).
- 689 68. S. Hamidi, Y. Nakaya, H. Nagai, C. Alev, T. Kasukawa, S. Chhabra, R. Lee, H. Niwa, A. Warmflash, T.
690 Shibata, G. Sheng, Mesenchymal-epithelial transition regulates initiation of pluripotency exit before
691 gastrulation. *Development (Cambridge)*. **147** (2020).
- 692 69. I. Barbaric, V. Biga, P. J. Gokhale, M. Jones, D. Stavish, A. Glen, D. Coca, P. W. Andrews, Time-lapse
693 analysis of human embryonic stem cells reveals multiple bottlenecks restricting colony formation and their
694 relief upon culture adaptation. *Stem Cell Reports*. **3**, 142–155 (2014).
- 695 70. S. Wakao, M. Kitada, Y. Kuroda, F. Ogura, T. Murakami, A. Niwa, M. Dezawa, Morphologic and Gene
696 Expression Criteria for Identifying Human Induced Pluripotent Stem Cells. *PLoS ONE*. **7** (2012).
- 697 71. M. Hashimoto, H. Sasaki, Epiblast Formation by TEAD-YAP-Dependent Expression of Pluripotency
698 Factors and Competitive Elimination of Unspecified Cells. *Developmental Cell*. **50**, 139-154.e5 (2019).
- 699 72. R. Levayer, C. Dupont, E. Moreno, Tissue Crowding Induces Caspase-Dependent Competition for Space.
700 *Current Biology*. **26**, 670–677 (2016).
- 701 73. J. Fadul, J. Rosenblatt, The forces and fates of extruding cells. *Current Opinion in Cell Biology*. **54**, 66–71
702 (2018).
- 703 74. E. Hannezo, C. P. Heisenberg, Mechanochemical Feedback Loops in Development and Disease. *Cell*. **178**,
704 12–25 (2019).
- 705 75. J. A. Halliwell, T. J. R. Frith, O. Laing, C. J. Price, O. J. Bower, D. Stavish, P. J. Gokhale, Z. Hewitt, S. F.
706 El-Khamisy, I. Barbaric, P. W. Andrews, Nucleosides Rescue Replication-Mediated Genome Instability of
707 Human Pluripotent Stem Cells. *Stem Cell Reports*. **14**, 1–9 (2020).

- 708 76. K. A. Knouse, K. E. Lopez, M. Bachofner, A. Amon, Chromosome Segregation Fidelity in Epithelia
709 Requires Tissue Architecture. *Cell*. **175**, 200-211.e13 (2018).
- 710 77. K. L. McKinley, N. Stuurman, L. A. Royer, C. Schartner, D. Castillo-Azofeifa, M. Delling, O. D. Klein,
711 R. D. Vale, Cellular aspect ratio and cell division mechanics underlie the patterning of cell progeny in
712 diverse mammalian epithelia. *eLife*. **7**, 1–20 (2018).
- 713 78. S. Singla, L. K. Iwamoto-Stohl, M. Zhu, M. Zernicka-Goetz, Autophagy-mediated apoptosis eliminates
714 aneuploid cells in a mouse model of chromosome mosaicism. *Nature communications*. **11**, 2958 (2020).

715

716

717 **ACKNOWLEDGMENTS**

718

719 **Funding** : This work was supported in part by funding grants from European commission H2020-EIC-SMEInst
720 (grant agreement number: 881113 C-stemGMP), iLAB2018 Bpi France, Region Nouvelle Aquitaine and Agence
721 Nationale pour la Recherche (ANR-17-C18-0026-02). We acknowledge the Bordeaux Imaging Center, a service
722 unit of the CNRS-INSERM and Bordeaux University, member of the national infrastructure France BioImaging
723 supported by the French Research Agency (ANR-10-INBS-04). We also acknowledge the TBMCORE facility.
724 (CNRS UMS 3427 – INSERM US 005). We also thank Nicolas Doulet and Marion Pilorge for helping build the
725 collaboration between Treefrog Therapeutics and the Imagine Institute.

726

727 **Author contributions** : KA NL MF designed the project and supervised experiments and analysis; PC performed
728 the experiments, analyzed the data and wrote the article; Experiments were performed both at the Imagine
729 Institute and at Treefrog Therapeutics (TFT). AL helped performing experiments, analysing the data and writing
730 the article; EL FM ML designed bioreactor cultures and scale-up, EL JP HW EJ MD performed bioreactor
731 cultures; JC EW EQ CB EP contributed to 2D cultures, encapsulations, trilineage assay and SNP analysis; BG
732 contributed to data analysis and writing.; PVL proposed a mathematical formulation for PDT and viability. PN

733 helped analyze the growth of 3D colonies and write the manuscript. KA CR JH conceived and produced the
734 microfluidic chips and performed high speed camera recordings.

735

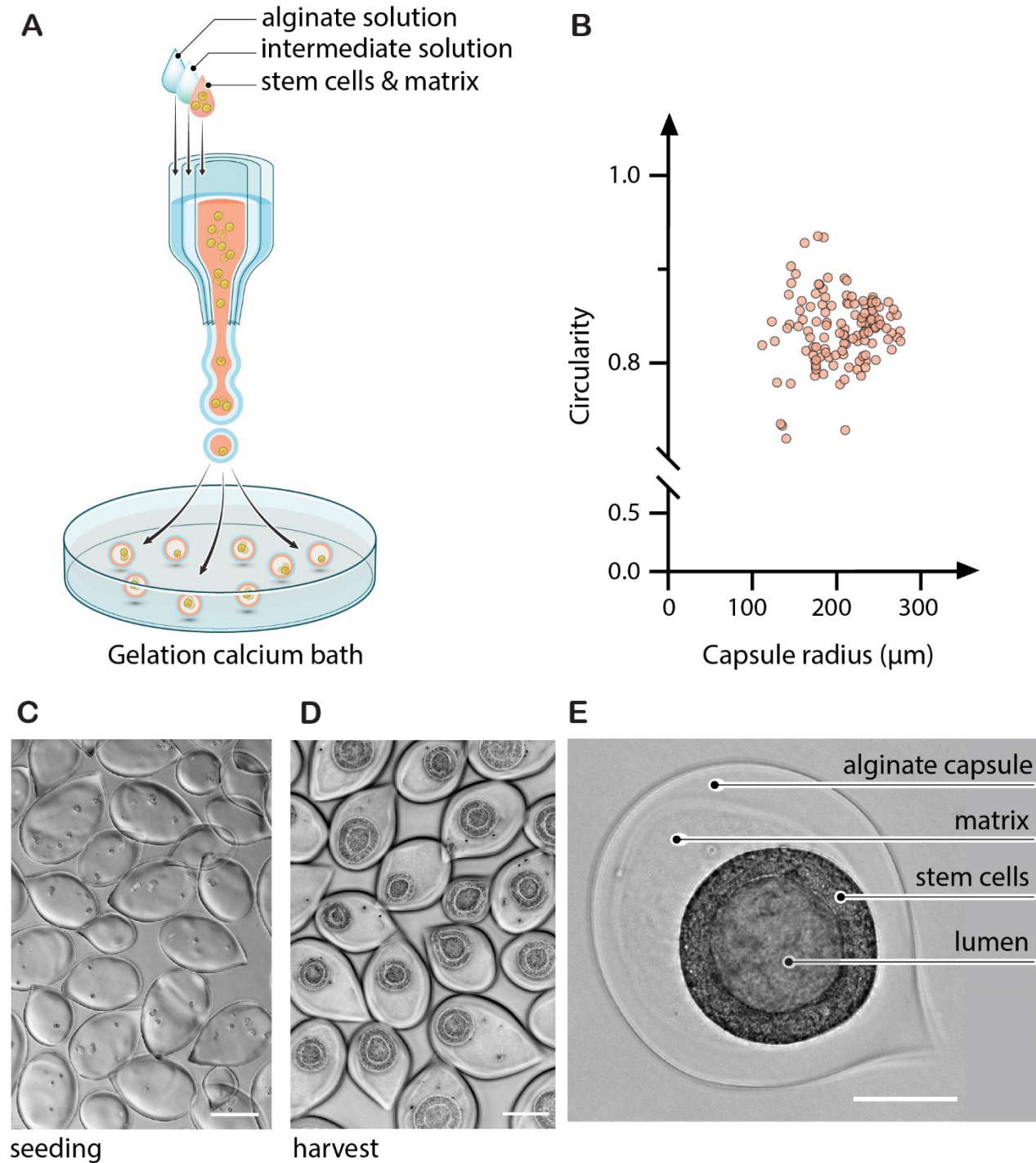
736 **Competing interests :** MF and KA are the founders of TFT; MF, KA, PC and PN are shareholders of Treefrog
737 therapeutics. MF KA and PN have a patent pertaining to discoveries presented in this manuscript. Patent no:
738 WO2018096277A1.

739

740 **Data and materials availability :** All data are available in the main text or the supplementary materials.

741 **FIGURES AND TABLES**

742

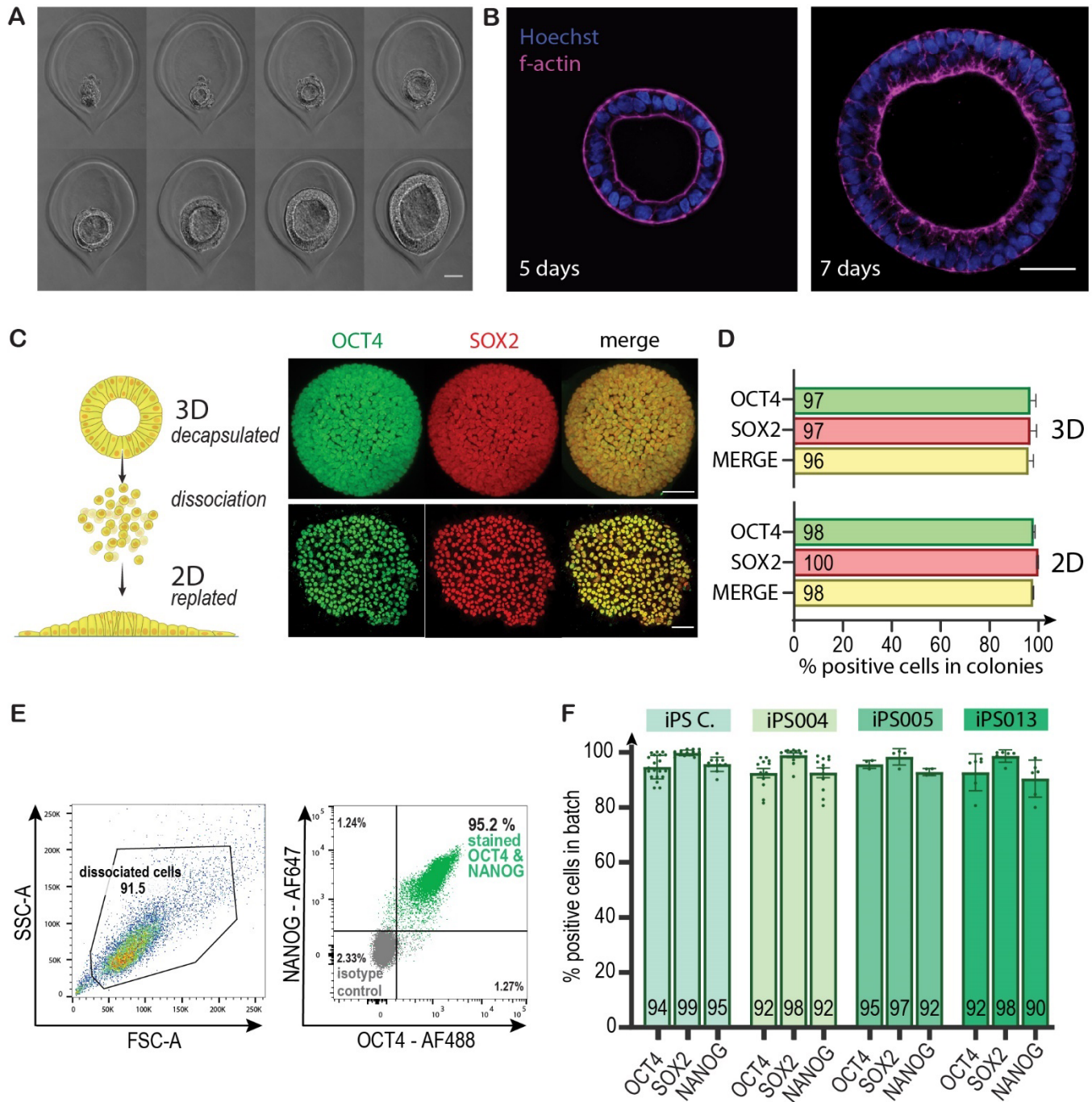


743

744

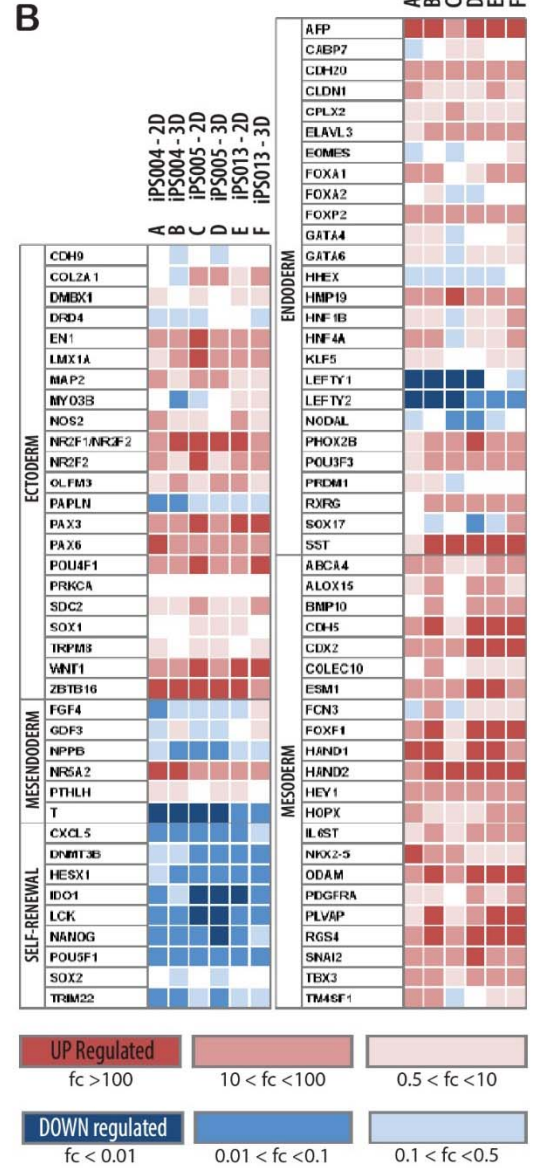
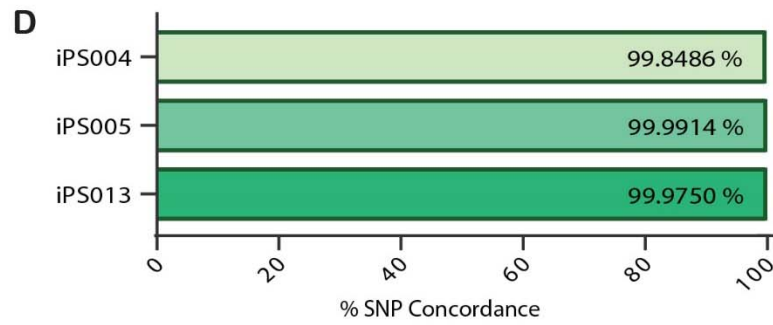
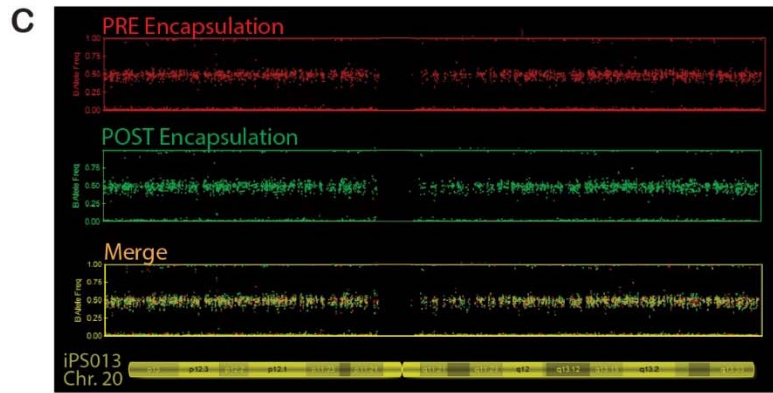
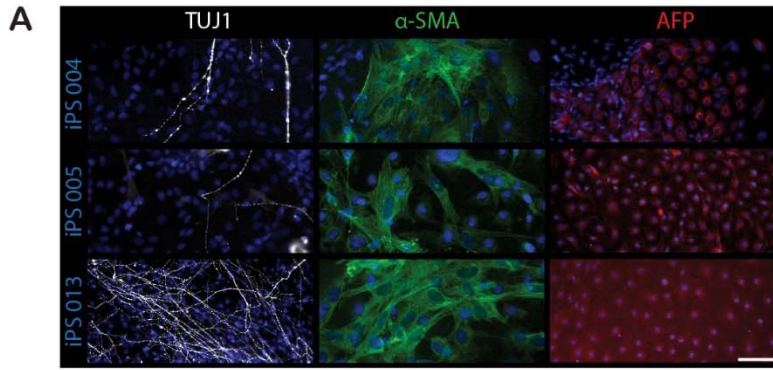
745 **Fig. 1. Encapsulation of human pluripotent stem cells (hPSCs) and suspension culture of 3D lumenized**
746 **colonies**

747 **(A)** Working principle of the microfluidic encapsulation technique. Co-extrusion of three co-axial flows generates
748 composite cell-and extracellular matrix (ECM)-laden droplets. The outer layer composed of alginate solution
749 undergoes gelation upon contact with a calcium bath. Cells are entrapped in the core-shell capsules and ECM
750 condensates onto the internal wall to form a niche-like environment. **(B)** Morphometric analysis of the capsules.
751 Graph of capsule circularity as a function of capsule radius for a representative batch of capsules (n=125). **(C-D)**
752 Phase contrast micrographs of the encapsulated hPSCs after seeding at day 0 (C) and before harvest at day 7 (D)
753 of the suspension culture course. Scale bar is 200 μ m. **(E)** Magnified phase contrast image showing the hollow
754 alginate capsule revealing the cyst architecture of the encapsulated hPSC colony. Scale bar=100 μ m.



757 **Fig. 2. Morphology, growth and stemness of *in capsulo* self-assembled 3D hPSC colonies**

758 (A) Snapshots of phase-contrast microscopy images showing the growth of an 3D hPSC colony. The time interval
759 between successive images is 12h. The scale bar is 50 μ m. (B) Confocal image of the equatorial plane of a hPSC
760 colony grown in a capsule at day 5 (left) and day 7 (right) cytoskeletal actin is stained in purple (Phalloidin) and
761 nuclei in blue (Hoechst). Scale bar=50 μ m. (C) Left: Cartoon explaining how 3D hPSC colonies are dissociated
762 and replated to form 2D colonies. Right: Immunostaining of a representative encapsulated 3D colony (upper
763 panel, scale bar=50 μ m) and a 2D colony obtained after replating (lower panel, scale bar=100 μ m): OCT4 (green)
764 SOX2 (red) and Merge (OCT4/SOX2). (D) Percentage of cells positive for markers of stemness among 4
765 representative colonies co-stained for OCT4 and SOX2 in 3D capsules (upper panel) and in 2D (lower panel).
766 Number of counted nuclei: n = 1159 for 3D and n=671 for 2D cells, see also Fig. S3). Error bars show the
767 standard deviation of the mean. (E) Flow cytometry dot-plots for stemness markers (OCT4 and NANOG) of a
768 batch of 3D hPSC colonies after 7 days of culture (T-Flask). (F) Histograms showing the percentage of OCT4,
769 SOX2 and NANOG positive cells in 3D hPSC colonies (culture in T-Flask) analyzed by flow cytometry at 7 days
770 post encapsulation for 4 iPS cell lines (with n \geq 3 independent biological replicates per cell line, n=42 total
771 number of experiments). Error bars represent the standard error of the mean.



772

773

774 **Fig. 3. Maintenance of pluripotency and genomic integrity in 3D hPSC colonies**

775 (A) Microscopy images of immunohistochemistry-based trilineage assay of 3 iPSC lines with 4 stainings: TUJ1

776 (White, early ectoderm), α -SMA (green, early mesoderm), AFP (Red, early endoderm), Dapi (Blue). (B)

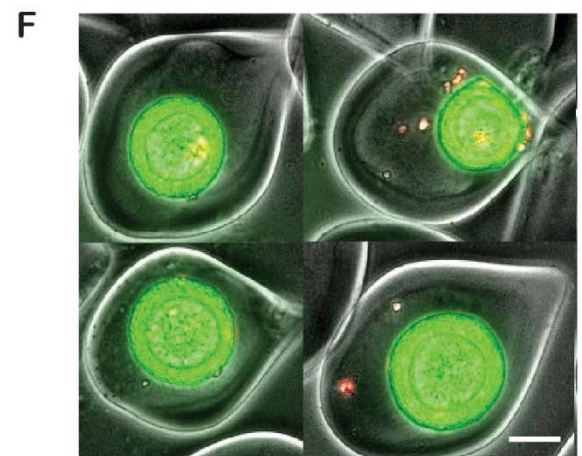
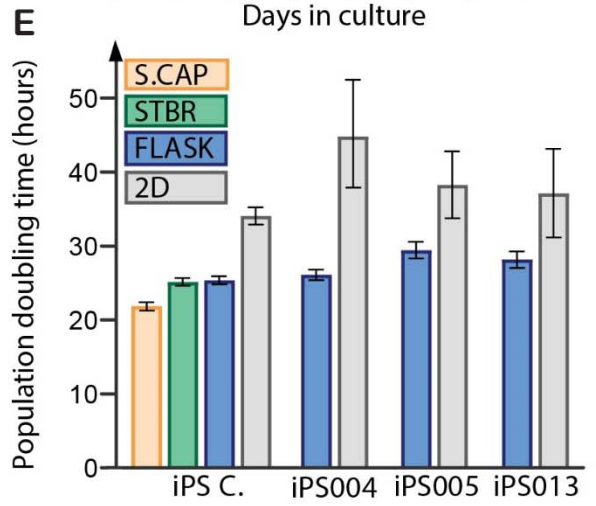
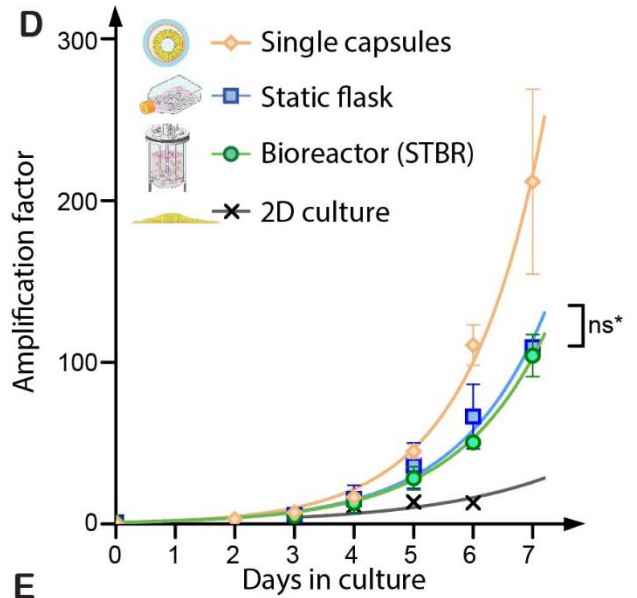
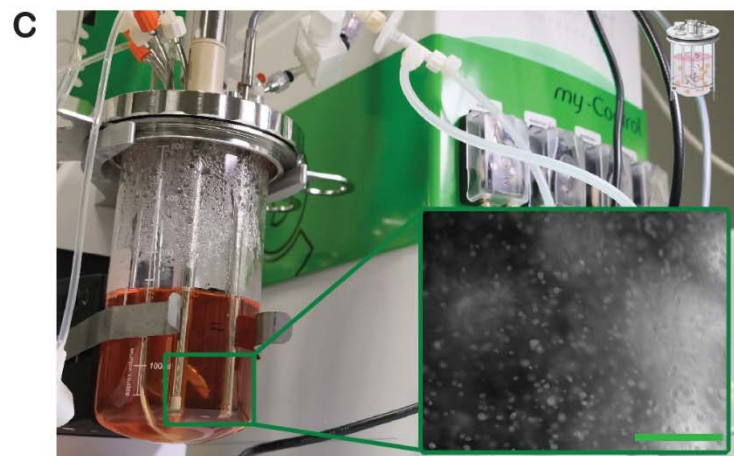
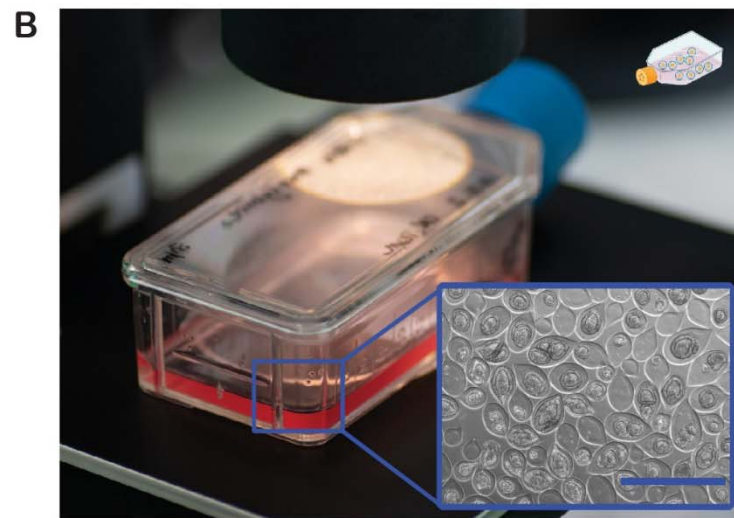
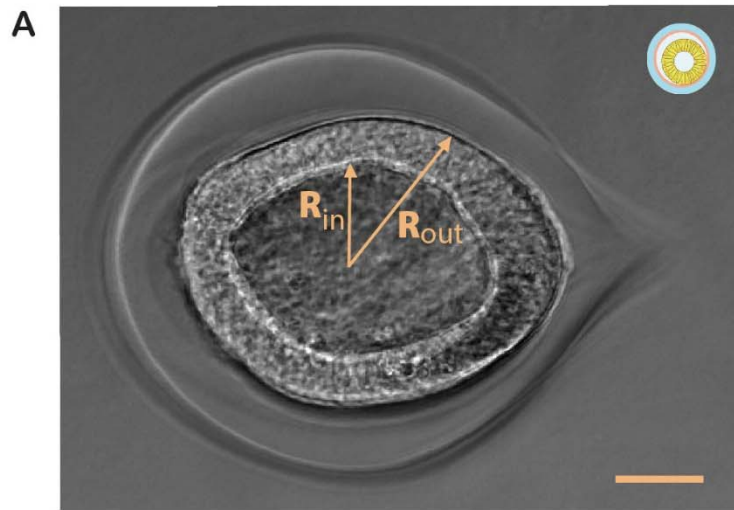
777 Scorecard™ differentiation assay comparing 3 iPS cell lines expanded in 2D and 3D encapsulated hPSC colonies.

778 (C) Comparison of high-resolution SNP arrays before and after one-week of encapsulation for iPS013 cell line :

779 Zoom on chromosome 20 for pre-encapsulation (red) and post-encapsulation (green). The merge (yellow) is

780 shown to highlight the absence of duplications and deletions. (D) Quantitative analysis yielding genotype SNP

781 concordance before and after one-week of amplification as encapsulated 3D colonies for 3 cell lines .

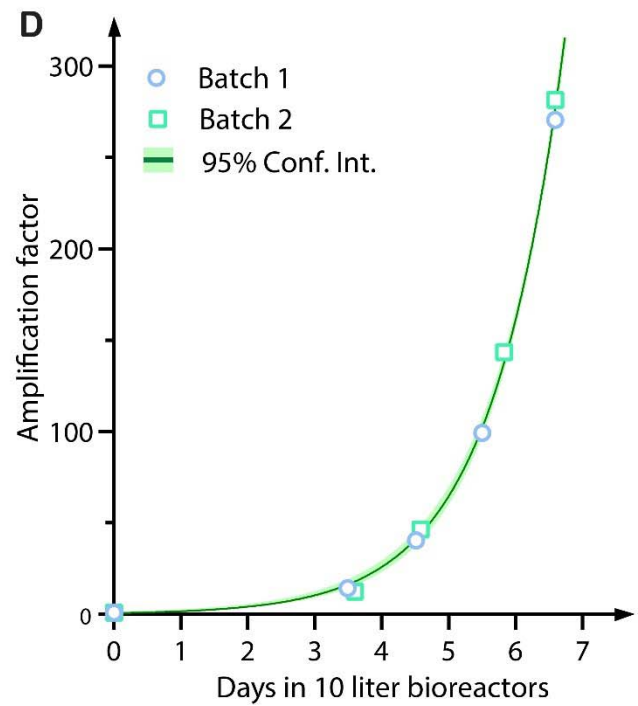
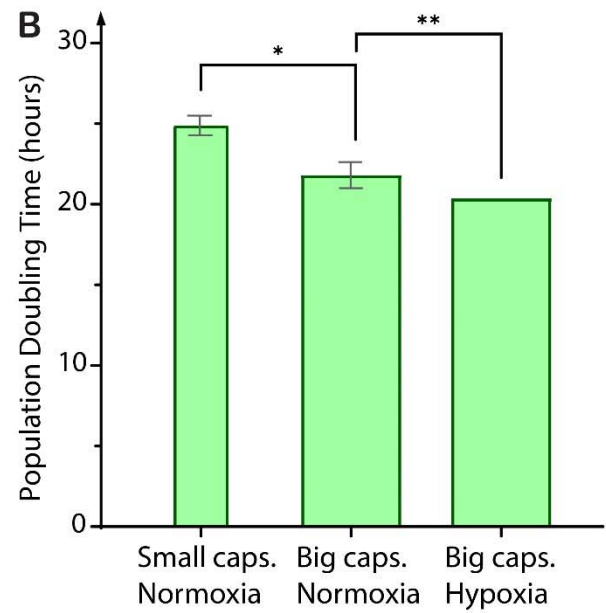
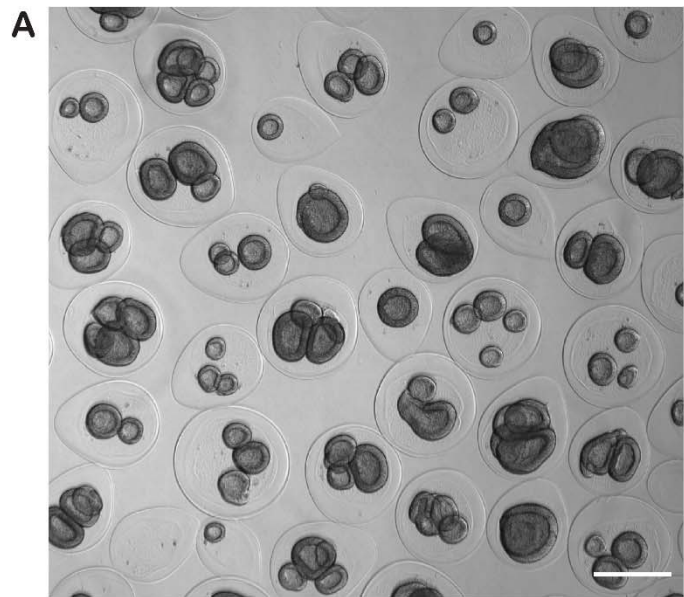


782

783

784 **Fig. 4. Amplification of 3D hiPSC colonies at the scale of a single capsule, in a static suspension and in**
785 **bioreactors**

786 (A) Micrograph of a 3D hPSC colony in a capsule and notations used in the next for the internal and external radii
787 of the cyst. (B) Static suspension culture of encapsulated 3D hPSCs. Insert : Phase contrast image showing 3D
788 hiPSCs colonies in capsules. Scale bar is 1000 μm . (C) Stirred suspension culture of encapsulated 3D hPSCs in a
789 500 ml benchtop STBR. Insert : Picture of the flowing capsules in the bioreactor. Scale bar is 4 mm. (D)
790 Amplification factor as a function of time for single capsules (orange, n= 6), static culture (blue, n=2), stirred
791 culture in a benchtop (volume 500ml) bioreactor (green, n=2), and conventional 2D cultures (grey). Last points in
792 the graph correspond to the harvest time. (E) Population doubling time of encapsulated hPSC colonies in single
793 capsules (S-CAP, orange), in a flask (FLASK, blue, n=42) and a benchtop bioreactor (STBR, green, n=2) and in
794 standard 2D cultures (2D, grey). Error bars represent the standard error of the mean. (F) Fluorescence microscopy
795 image of 4 representative encapsulated 3D hPSC colonies stained with Live/dead (green/red)). Scale bar is 100
796 μm . All data shown here were obtained with iPS C line, except panel 4D that collects data for the 4 available cell
797 lines.

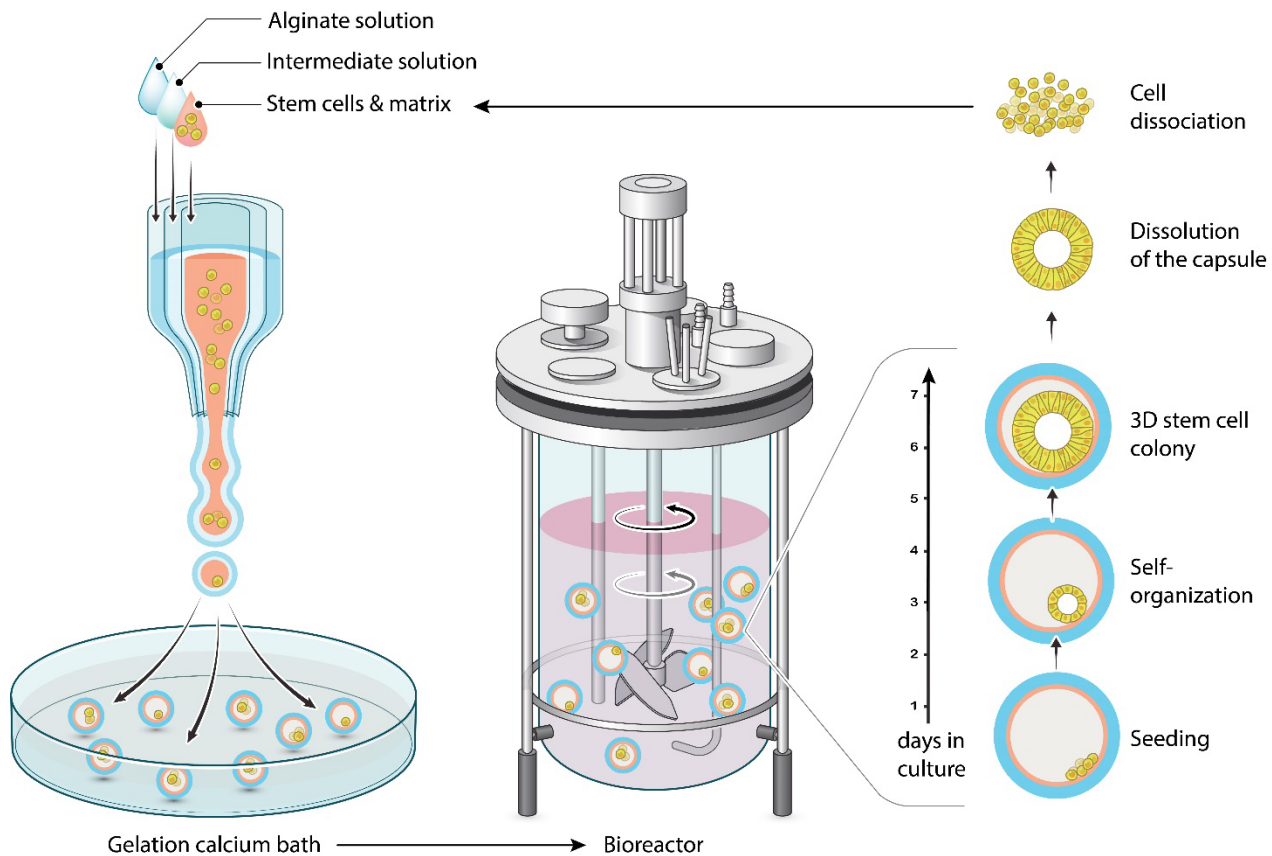


798

799

800 **Fig. 5. Impact of capsule size and oxygen tension on hPSC amplification and scalability in stirred tank**
801 **bioreactors**

802 (A) Phase contrast image showing 3D hiPSCs colonies in capsules referred to as “big” in the main text (with an
803 average radius of 300µm). Scale bar = 500µm. (B) Population doubling time of encapsulated 3D hiPSCs colonies
804 cultivated in benchtop bioreactors by varying the size of the capsules and the oxygen tension conditions
805 (normoxic versus hypoxic). Mean and standard deviation (* p<0,001 and ** p <0,01). (C) Picture of a 10 liter
806 industrial stirred tank bioreactor used to test the scalability of the stem cell capsule culture system. (D) Graph of
807 amplification factor of hiPSCs grown in 10 liter bioreactors over a week, in ‘Big capsules’ and hypoxic
808 conditions; Data were obtained from 2 independent batches and from 2 independent encapsulations. Light green
809 band shows the 95% confidence interval of the fitting curve.



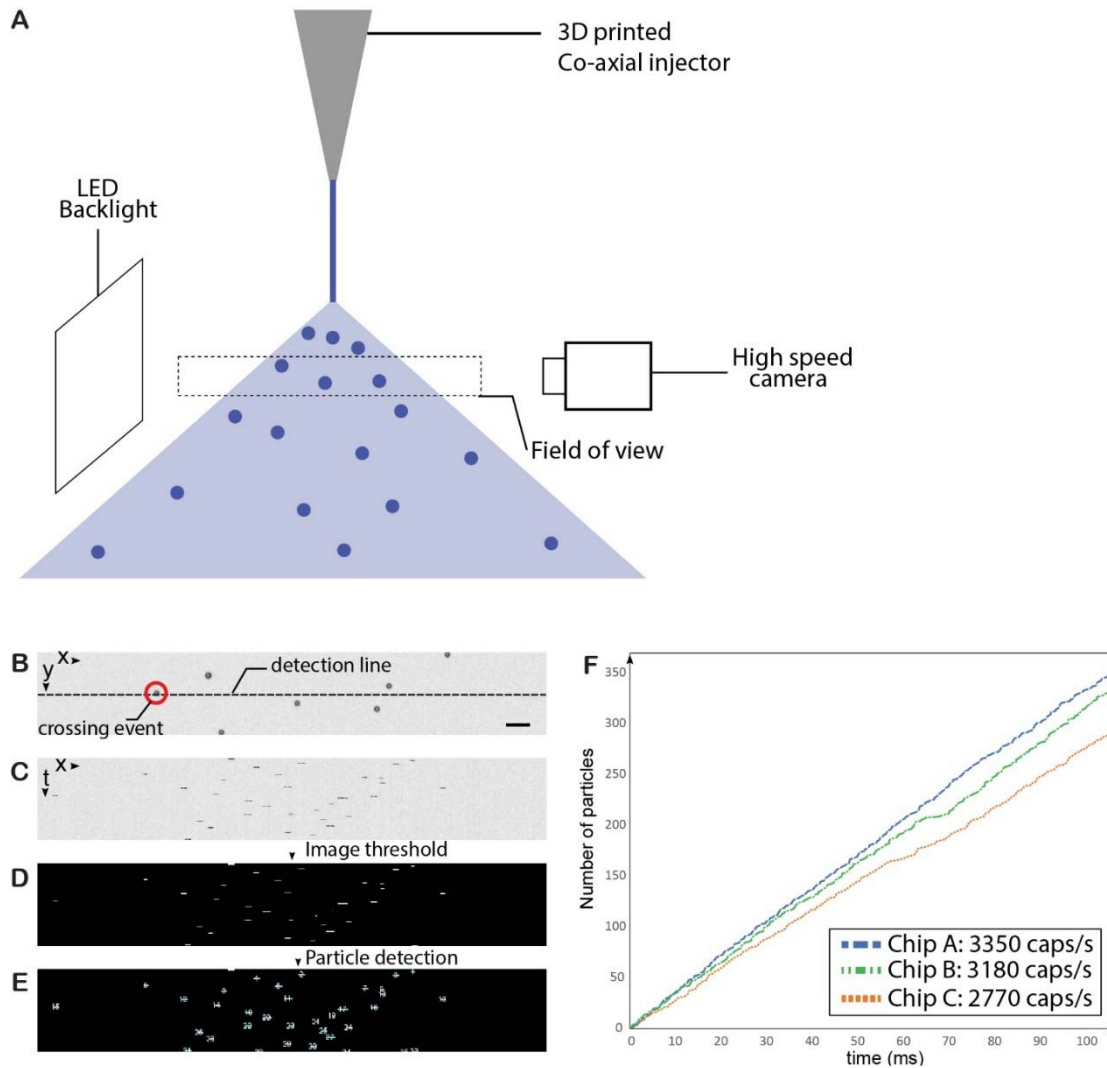
810
811

812

813 **Fig. 6. C-STEM pipeline: encapsulation and scale-independent culture of encapsulated 3D hPSC colonies in**
814 **bioreactors**

815 After encapsulation using the microfluidic extrusion technique (left panel), hPSC in matrix-laden capsules are
816 transferred to suspension culture in a bioreactor (middle panel). Under controlled conditions provided by the
817 bioreactor, hPSC cells self-organize into cysts which are protected by the capsules. These growing 3D colonies
818 are harvested and dissociated after capsule dissolution. Subsequent cell suspension may then serve for another
819 encapsulation and expansion.

820 SUPPLEMENTARY MATERIAL

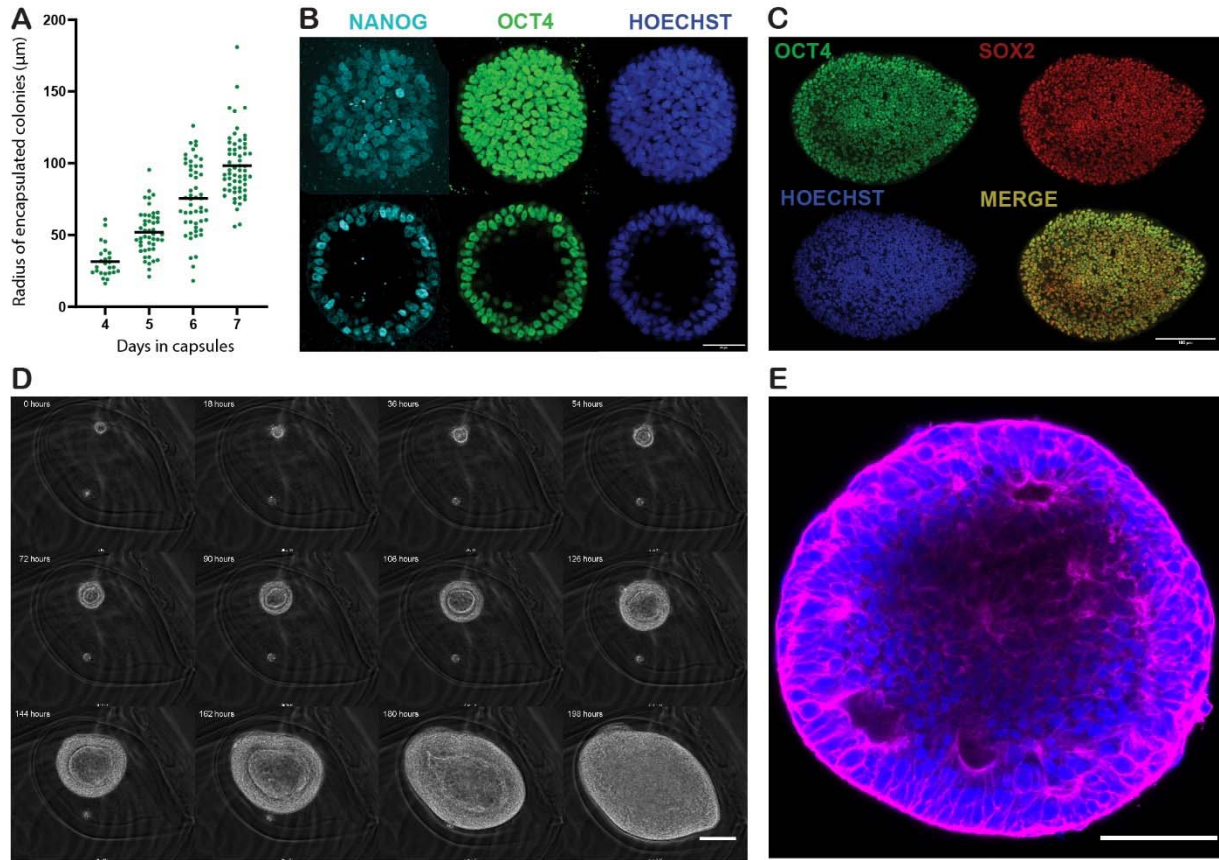


821

822

823 **Fig. S1. Optical measurement of the capsule production rate.**

824 (A) Sketch of the experimental setup. The capsules exiting the nozzle are illuminated with a LED
825 backlight (PHLOX 200mx200mm) and imaged using a high-speed camera (HSC Phantom VEO1310L)
826 at a frame rate of 10,000 fps and a spatial resolution is 30px/mm. (B) Snapshot showing a typical
827 shadow image of the capsule spray. Scale bar is 1mm. The algorithm increments the account of counts
828 capsules every time one of them crosses the detection line (dashed-white in (b)), and stores the time of
829 the event. Details of the detection algorithm are shown proposed in (c-e). (C) Space-time representation
830 of the crossing events, evidenced by stacking the intensity variations of the detection line over time.
831 Each crossing event corresponds to a black spot in the image. (D) Intensity threshold of (c). Elementary
832 binary operations are performed to ensure that each crossing event corresponds to a single white spot.
833 (E) Particle analysis (using ImageJ plugin). Each white spot is counted independently, and its
834 coordinates are stored by the algorithm, providing details on the time and location of the crossing event.
835 (F) Example of typical production curves for three different spraying nozzles (chips A, B and C). The
836 corresponding production rates are included in the legend. The values are usually estimated with longer
837 datasets (recordings >500 ms).

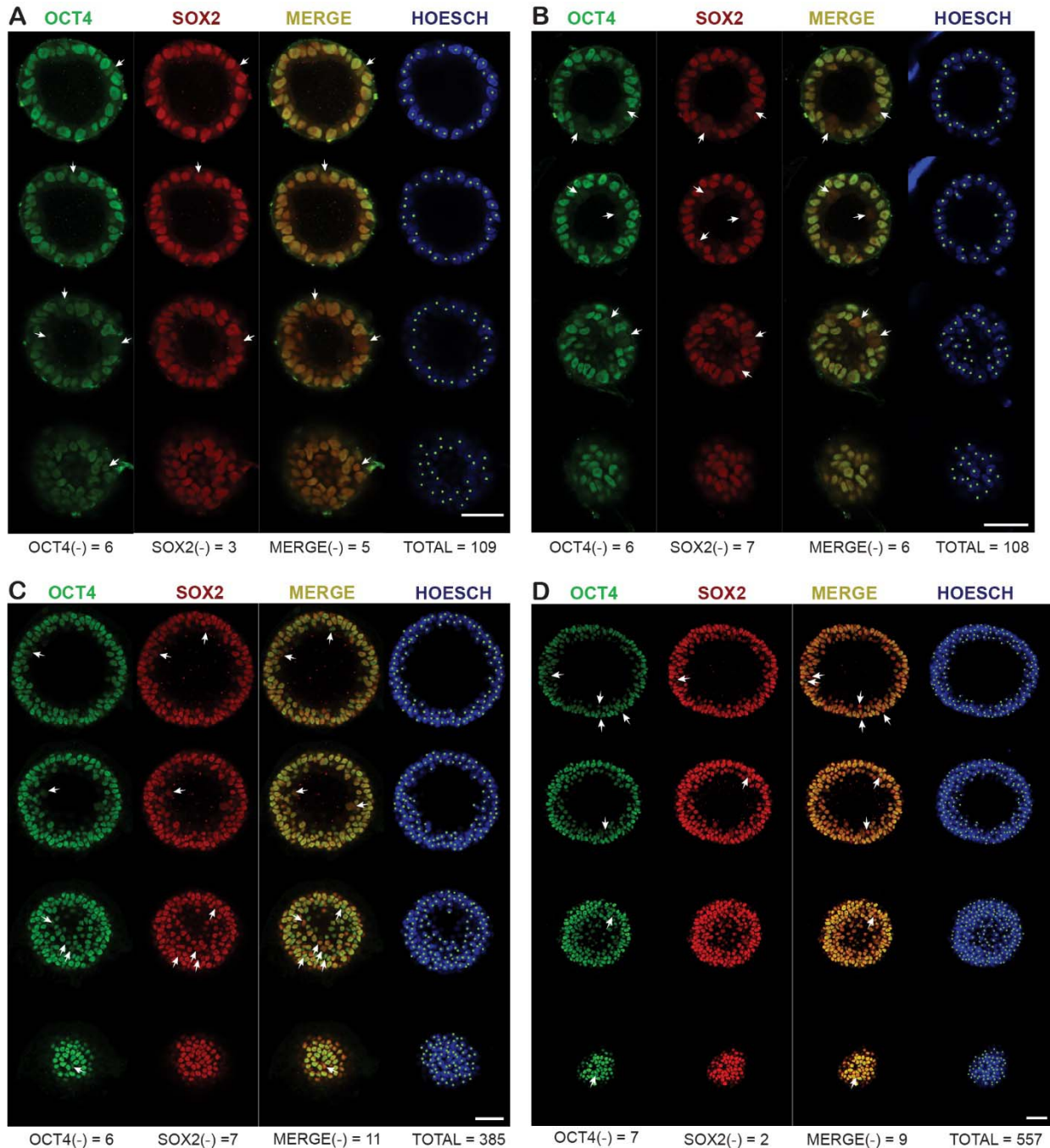


838

839

840 **Fig. S2. Phenotype of encapsulated 3D hPSC colonies**

841 (A) Graph of hPSC cyst radius as a function of time. Radii were measured by monitoring n=25, 47, 52,
842 61 capsules at days 4, 5, 6 and 7 respectively. (B) 3D hPSC colony co-stained for stemness markers
843 NANOG (cyan) and OCT4 (green) and with Hoechst (blue). Projection of maxima (upper panel) and
844 equatorial plane (lower panel) of confocal images. Scale bar is 50μm. (C) Confocal equatorial plane of a
845 fully confluent hPSC capsule (t=10 days post-encapsulation) co-stained for OCT4 (green), SOX2 (red),
846 and nuclei (Hoechst, blue) and showing that the lumen has collapsed. Scale bar is 100μm. (D) Sequence
847 of phase-contrast microscopy images showing luminogenesis, growth and collapse of an encapsulated
848 epiblast-like colony. The time interval between successive images is 18h. Scale bar=100μm. (E)
849 Confocal equatorial plane of a collapsed 3D hPSC colony co-stained for F-actin (Phalloidin, magenta)
850 and nuclei (Hoechst, blue), Scale bar=100μm.



851

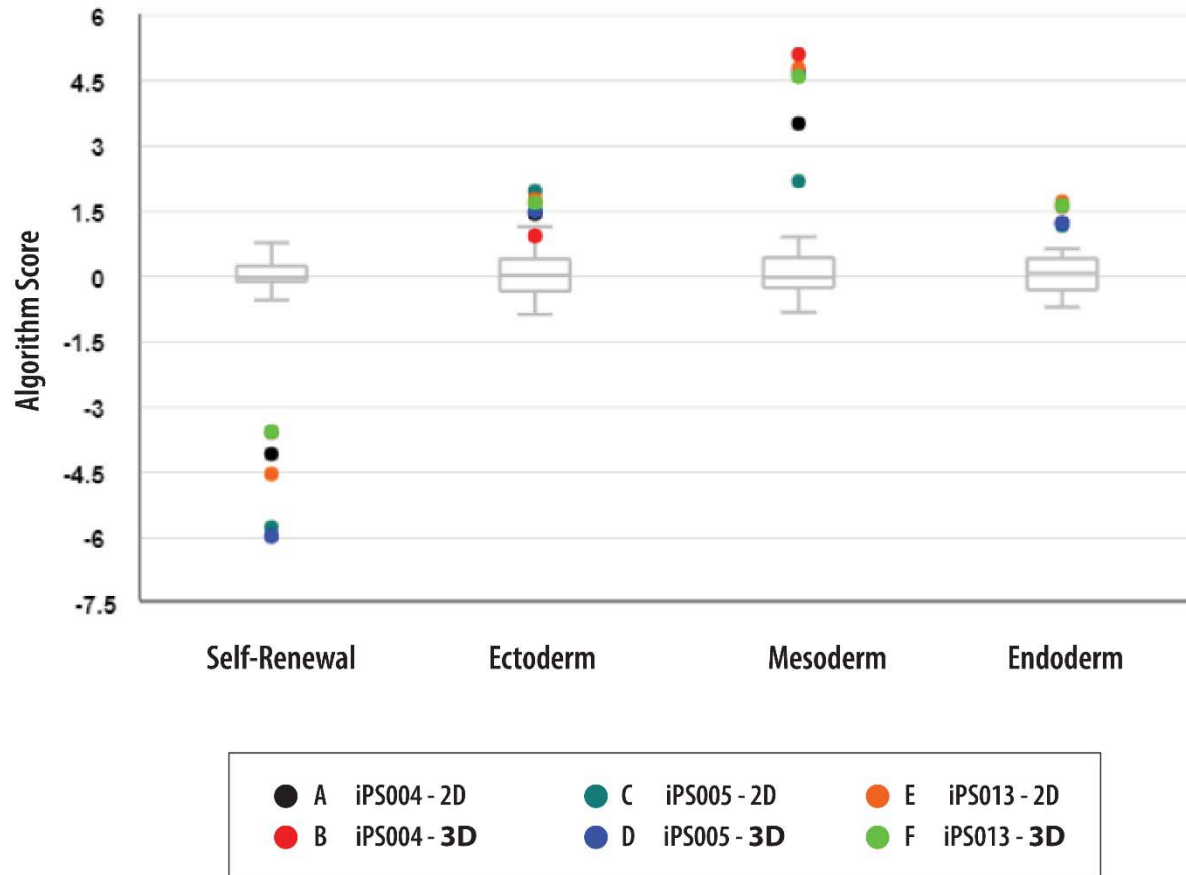
852

Fig. S3. Stemness staining of encapsulated 3D hPSC colonies

853

Four different representative encapsulated hPSC colonies co-stained for OCT4 (green) SOX2 (red) and nuclei (Hoechst, blue). The 2 colonies in the upper panels (A) and (B) are collected at day 5. The 2 colonies in the lower panels (C) and (D) are collected at day7. White arrows and dots illustrate the quantification method used to determine OCT4 (green) and SOX2 (red) co-staining and the percentage of positive cells within the encapsulated cysts shown in Figure 2D of the main text. Scale bars are 50 μm .

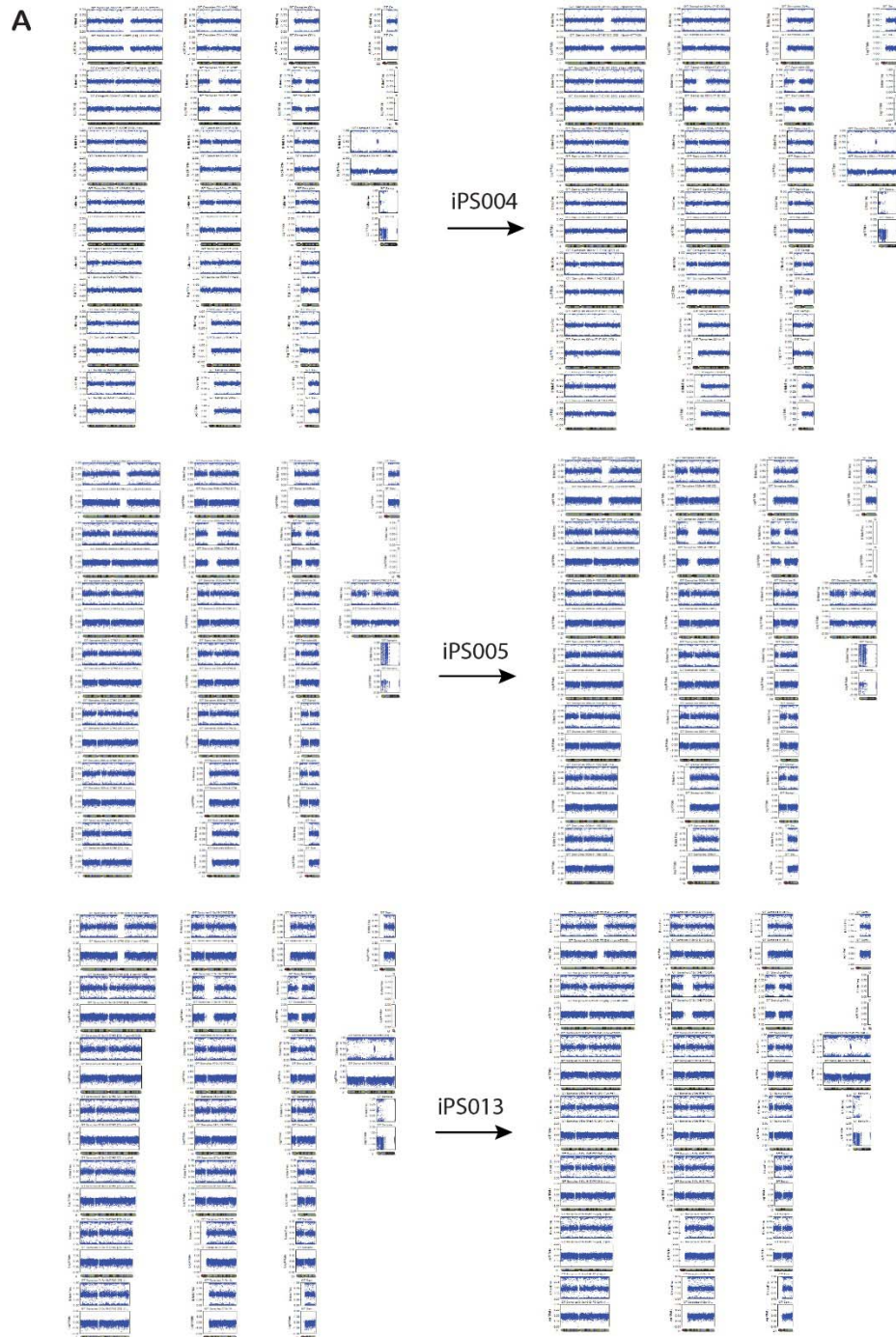
854
855
856
857
858



859
860

861 **Fig. S4. Scorecard quantitative comparison of gene expression profiles from trilineage**
862 **differentiation assays of 2D and 3D hPSC colonies**

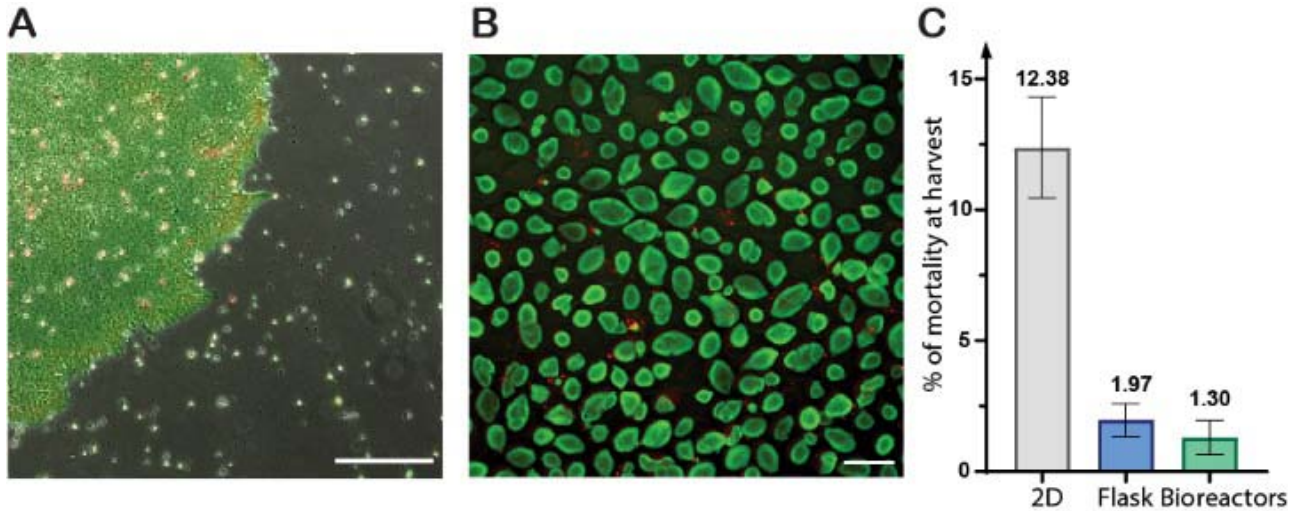
863 2D cultures and 3D *in capsulo* cultures of hPSC were assessed with trilineage differentiation assay and
864 scorecard qPCR panel. Three iPSC lines were differentiated and analyzed. Algorithm score generated by
865 the manufacturer confirm a consistent decreased of the self-renewal genes compared to the
866 undifferentiated reference. Up-regulation of the 3 germs layers means that both 2D and 3D stem cell
867 colonies can engage in differentiation. The grey box plot indicates the undifferentiated reference.



B

	Concordance of SNP Pre vs Post encapsulation			
	% concordance	Number of match	Informative SNP	Total SNP
iPS004	99,849%	304066	304527	305445
iPS005	99,991%	302217	302243	305445
iPS013	99,975%	300471	300546	305445

870 **Fig. S5. Analysis of high-resolution SNP arrays before and after C-STEM amplification**
871 (A) Qualitative analysis of high-resolution SNP arrays before and after one-week of encapsulation: pre-
872 encapsulation (left) and post-encapsulation (right). Absence of duplications and deletions for the 3
873 distinct iPS cell lines (iPS004 top row, iPS005 middle row, iPS013 lower row). (B) Table summarizing
874 the SNP concordance analysis.



875

876

Fig. S6. Cell viability in 2D and encapsulated 3D hPSC cultures

877

(A) Fluorescence microscopy image of a 2D stem cell colony stained for live (Calcein, green) and dead (ethidium, red). Pictures were taken before daily media changes to avoid removal of free-floating cells.

878

Scale bar is 500 μm . (B) Fluorescence microscopy image of live (green) & dead (red) staining of 3D

879

hPSC colonies at day 7 post encapsulation. Scale bar is 500 μm . (C) Percentage of cell mortality at

880

harvest for 2D culture and encapsulated 3D hPSC colonies. Stem cells cultivated in 2D were harvested

881

at day 4, 5 or 6 before reaching confluency. Stem cells cultivated for 6 to 7 days in capsules were

882

harvested and dissociated after capsule dissolution. Viability was assessed with Nucleo counter NC3000.

883

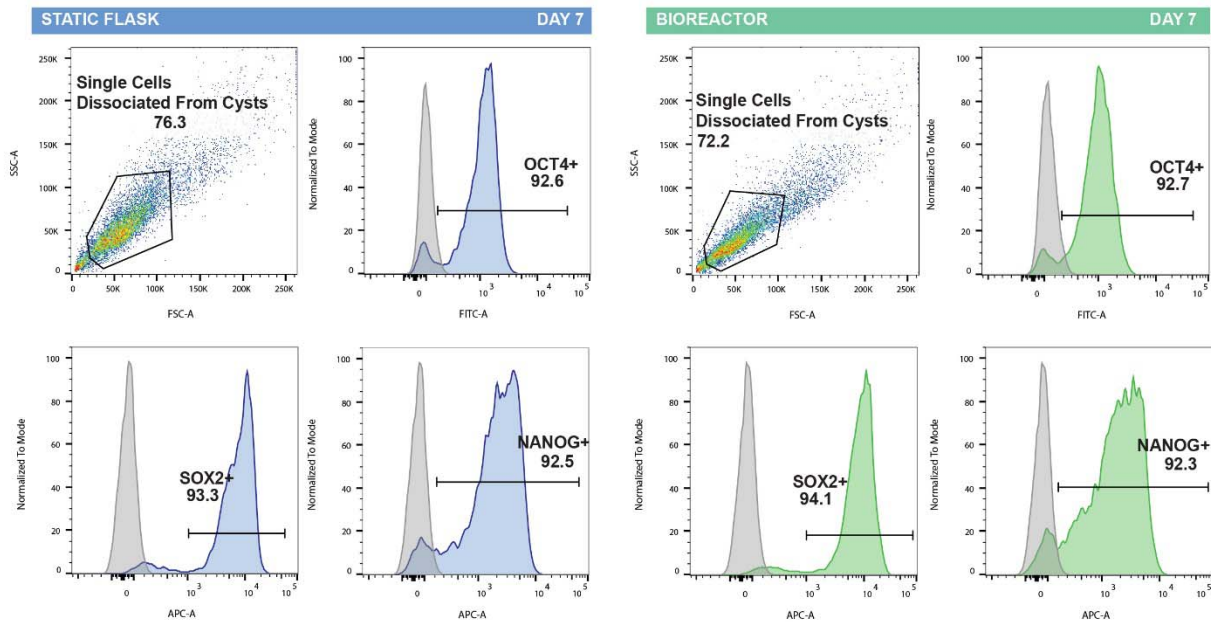
The 'count and viability assay' use the cell stain Acridine Orange for cell detection, and the nucleic acid

884

stain DAPI for detecting non-viable cells.

885

886



887

888

Fig. S7. Encapsulated epiblast-like colonies resilience to hydrodynamic damages

889

From one encapsulation batch, 2 suspension cultures were seeded in parallel: capsules were cultivated either in static suspension (flasks) or in constantly agitated suspension (500ml stirred tank bioreactor). after 7 days of suspension culture, capsules were collected, dissolved; 3D stem cell colonies were dissociated, fixed and stained for stem cell markers OCT4, SOX2 and NANOG. Fig. S7 shows flow cytometry dot-plots of the two different culture conditions (static flask versus stirred suspension in a bioreactor)

890

891

892

893

894

895

10L Batch n°1					
Target Oxygen Level	20% DO	hPSC seeded	56 millions	Viability at harvest	99,5 %
Max working volume	10.2 L	hPSC produced	15.2 billions	OCT4+ at harvest	92.0 %
Min % Capsule Volume	4,5 - 15%	Amplification factor	x271/ 6.59 days	SOX2+ at harvest	99.6 %
Max Cells / ml of Capsules	33,92 m/ml	Population Doubling Time	19.4 hours	NANOG+ at harvest	97.0 %
		Population Doubling Level	8.08		

10L Batch n°2					
Target Oxygen Level	20% DO	hPSC seeded	51 millions	Viability at harvest	99,7 %
Max working volume	9.7 L	hPSC produced	14.52 billions	OCT4+ at harvest	96.7 %
Min % Capsule Volume	3,9 - 14 %	Amplification factor	x282/ 6.69 days	SOX2+ at harvest	99.7 %
Max Cells / ml of Capsules	33.80 m/ml	Population Doubling Time	19.73 hours	NANOG+ at harvest	98.4 %
		Population Doubling Level	8.14		

896
897

898

Fig. S8. Key parameters and results of C-STEM scale-up in 10 liter bioreactor

899

900

901

902

903

904

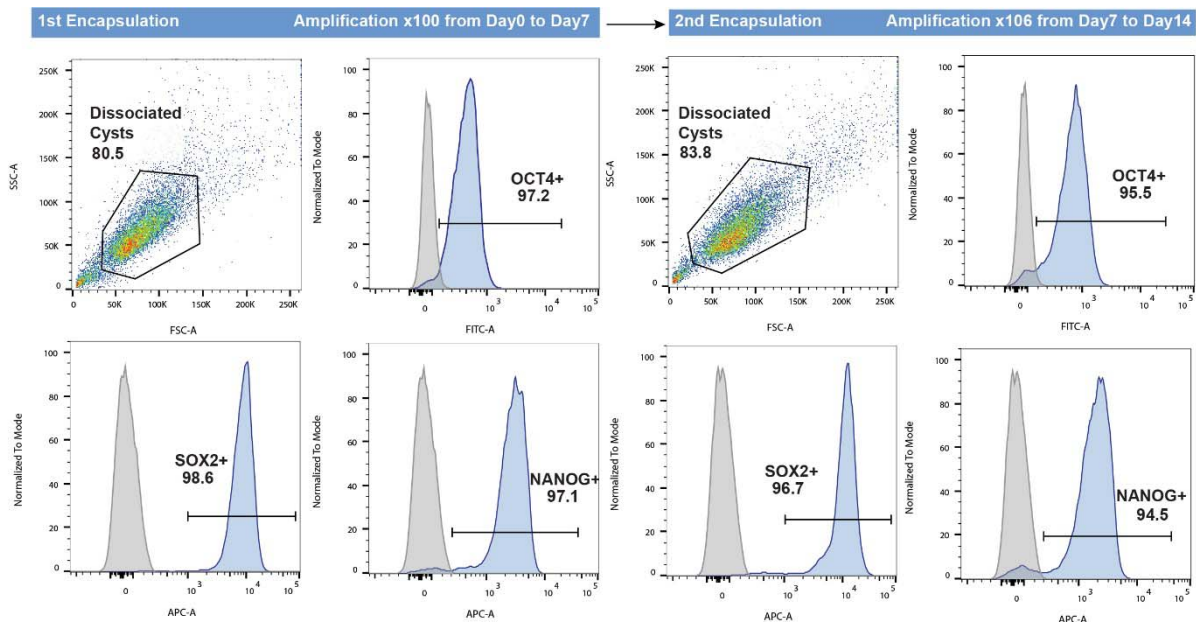
905

906

907

908

Encapsulation of hiPSCs and suspension culture was performed for 2 separated runs. Target oxygen level of 20% Dissolved Oxygen is described as a hypoxic condition (conversely to bioreactors with 100% dissolved oxygen level that are described as normoxic). A fed batch feeding strategy was applied resulting in increasing working volume and decreasing capsule concentration. The cell density can be expressed in millions of cells per milliliter of capsules. The volume of capsule harvested being measured in graduated glass cylinder and reported to the cell quantity. Amplification factor (AF), and Population doubling time (PDT) are defined following main text description. Population doubling level (PDL) is defined as $PDL(Dt) = \ln(AF) / \ln(2)$. Viability was assessed by nucleocounter NC-3000 (Chemometech). Decapsulated and dissociated cells were fixed and stained for OCT4, SOX2 and NANOG and analyzed by flowcytometry, BD Accuri C6 plus (Table S1).



909

910

Fig. S9. Stemness maintenance assessment of hiPSCs through 2 consecutive encapsulations

911

After a first encapsulation of hiPSCs and 7 days of suspension culture, capsules were collected and dissolved, and 3D colonies were dissociated, resuspended and used for another round of encapsulation/suspension culture. At day 7 and 14 cells were dissociated, fixed, and stained for the stemness markers OCT4, SOX2, and NANOG. Individual histograms from flow cytometry show stable phenotypes.

915

916 **MOVIE S1. Formation and collection of capsules in calcium bath.**

917 Video taken with a high speed camera showing how the train of droplets splays during the encapsulation
918 process under electric field. Acquisition was performed at a frame rate of 10.000 fps. Scale bar is 1mm.

919
920 **MOVIE S2. 3D rendering of an equatorially sectioned 3D hPSC colony.**

921 The image shows nuclear localization of OCT4 (green) and phalloidin (gray). The diameter of the cyst is
922 110 μm .

923

924 **MOVIE S3. Time-lapse of an encapsulated 3D hPSC colony : between encapsulation and harvest**

925 Phase contrast sequence (using Biostation Nikon IM) of a growing hPSC colony inside a capsule. Video
926 starts at day 1 after encapsulation. Scale bar is 100 μm .

927

928 **MOVIE S4. Time-lapse of an encapsulated 3D hPSC colony : between encapsulation and lumen**
929 **collapse**

930 Phase contrast sequence (using Biostation Nikon IM) of a growing hPSC colony inside a capsule. Video
931 starts at day 1 after encapsulation, prolonged until full collapse of the lumen. Scale bar is 100 μm .

932

933 **MOVIE S5. Encapsulated 3D hPSCs colonies cultured in a 10 liter stirred-tank bioreactor.**

934 Video taken with a Digital Single-Lens Reflex camera shows the flow of hPSC-laden capsules induced
935 by the motion of the bioreactor's impeller.

936 **Table S1. Antibody list**

937 List of antibodies used for flow cytometry, trilineage assay and immune fluorescence microscopy.

938

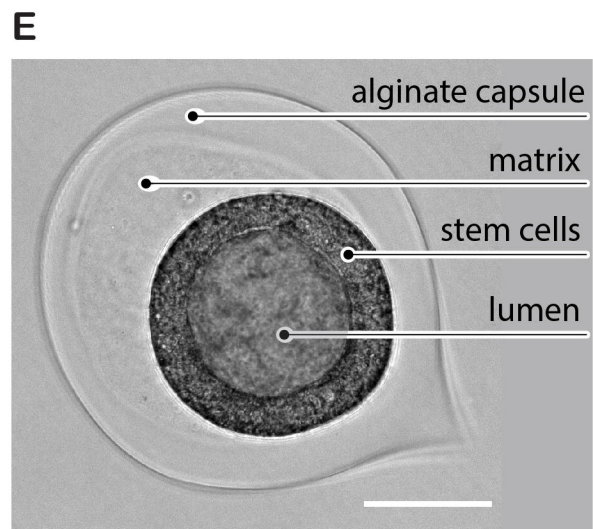
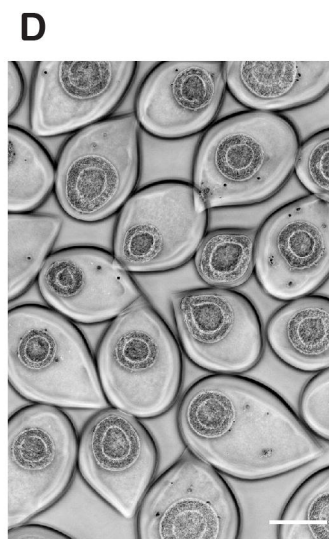
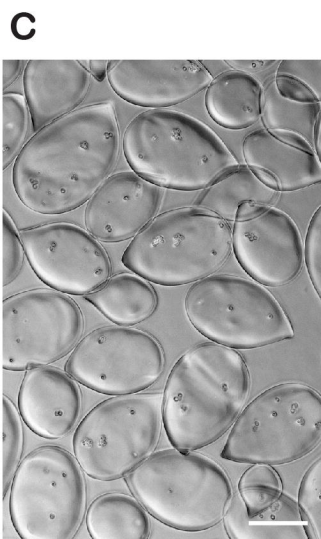
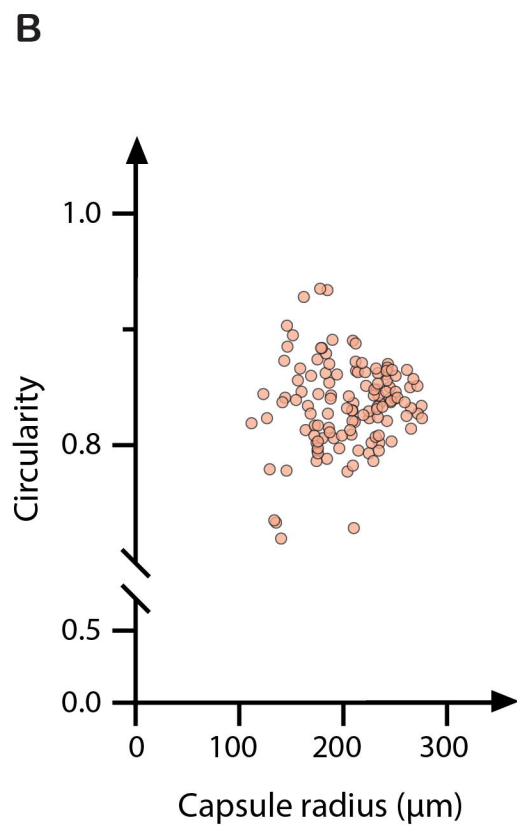
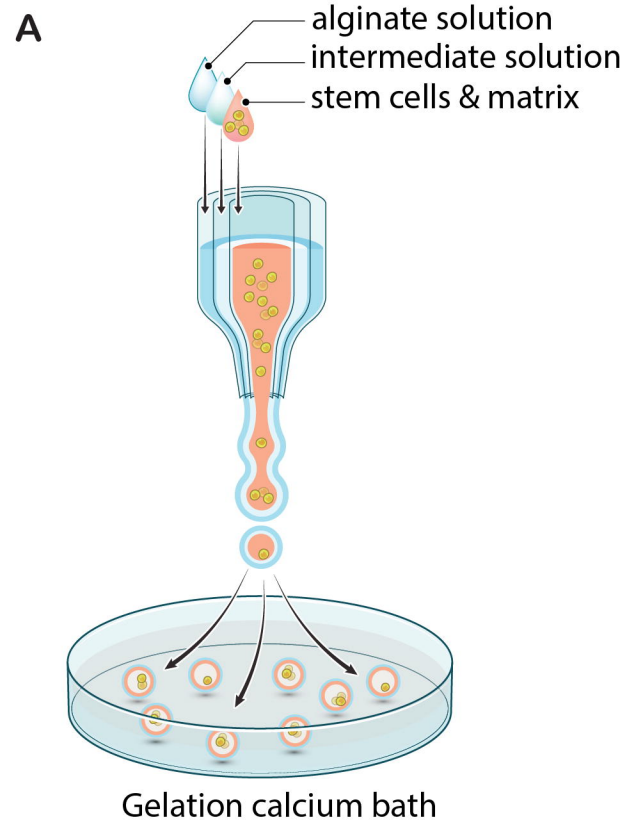
Antibodies used for flow cytometry	
Nanog Hu – Alexa Fluor647 Clone N3-355	BD (Ref. 561300)
OCT3/4 Hu, Ms – Alexa Fluor 488 – clone 40/oct3	BD (Ref. 560253)
SOX2 Hu Alexa Fluor 647 – Clone O30-678	BD (Ref. 562139)
Mouse igG1k – Alexa Fluor 488 – clone MOPC 21	BD (Ref. 557721)
Mouse igG1k, Alexa Fluor 647 clone MOPC 21	BD (Ref. 557732)

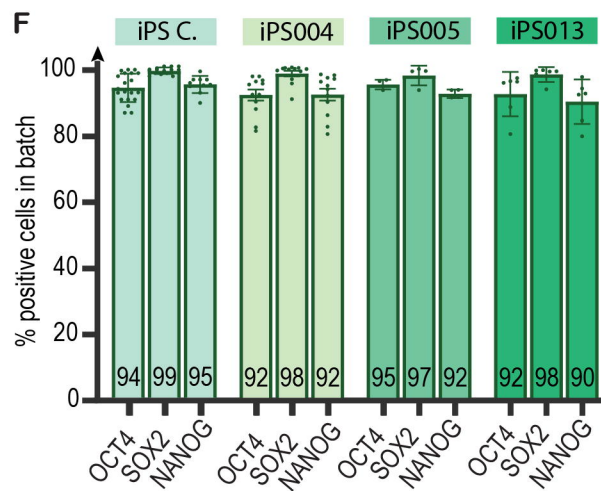
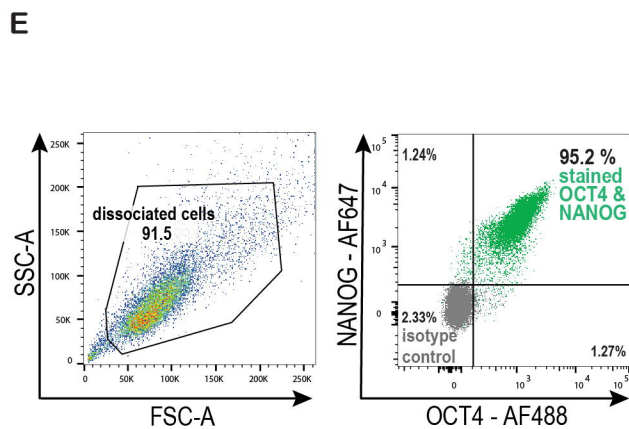
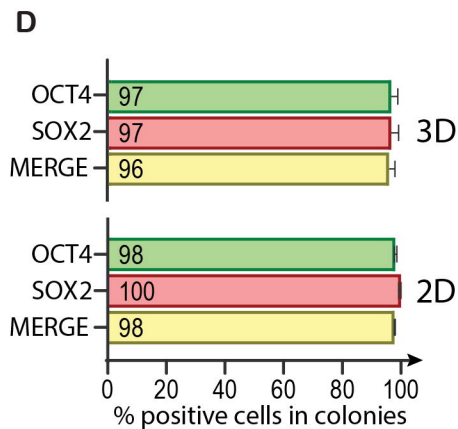
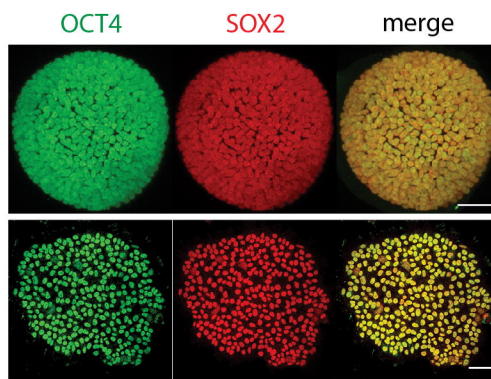
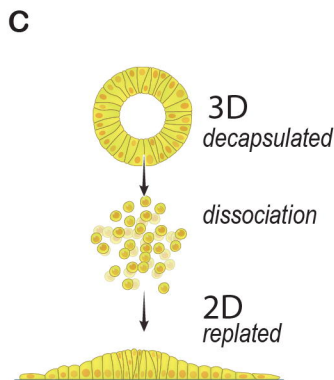
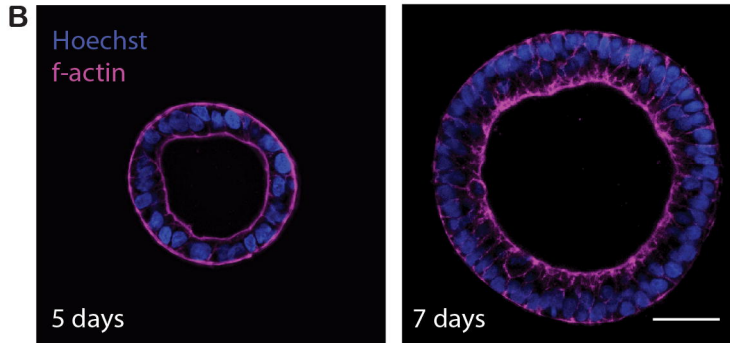
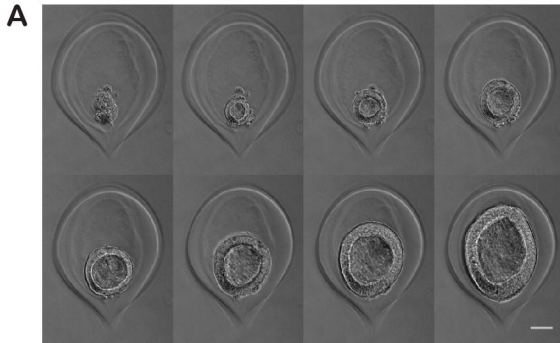
939

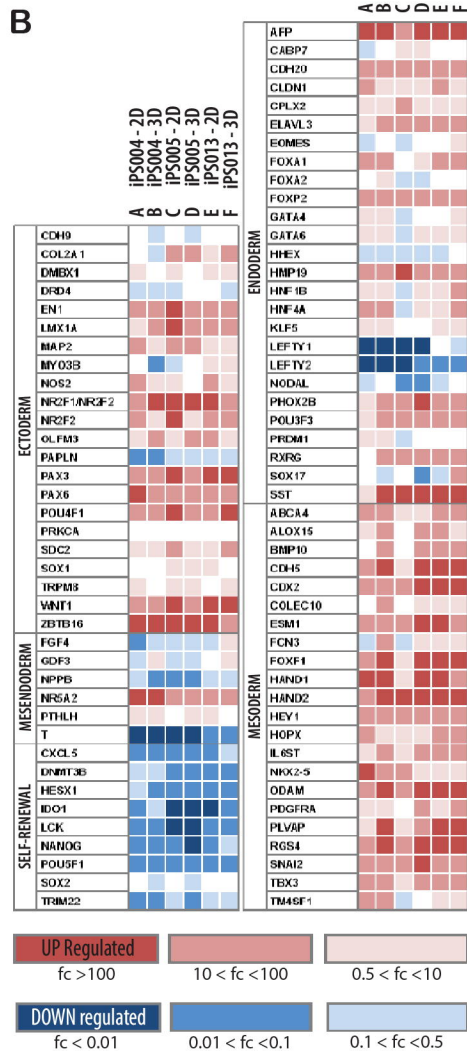
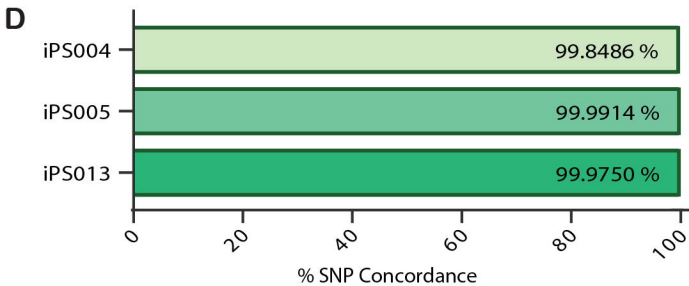
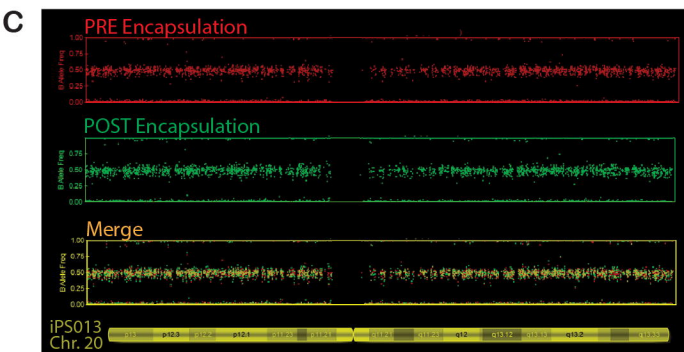
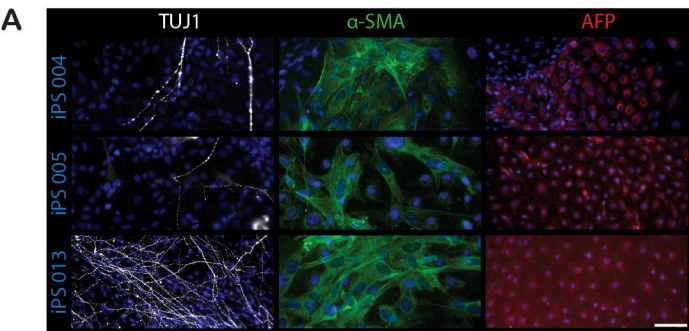
Antibodies used for trilineage assay	
Monoclonal anti-Tubuline beta 3 (Mouse) 1:1000	Biolegend Cat#801202
Monoclonal anti actin, alpha-smooth muscle (Mouse) – FITC 1:300	Sigma-Aldrich Cat#F3777
Monoclonal anti-Alpha foeto protein (Mouse) 1:60	R&D system Cat#MAB1369
Goat anti-Mouse alexa Fluor plus 555 1:1000	Thermo fisher Scientific Cat#A32732

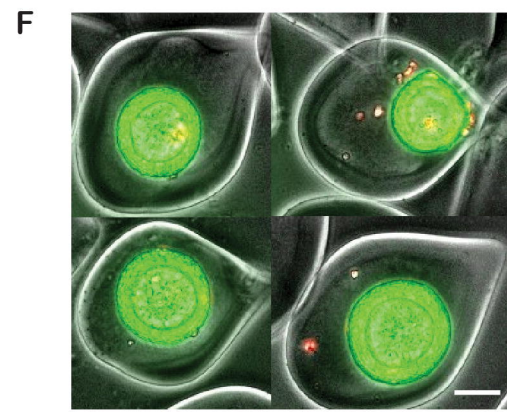
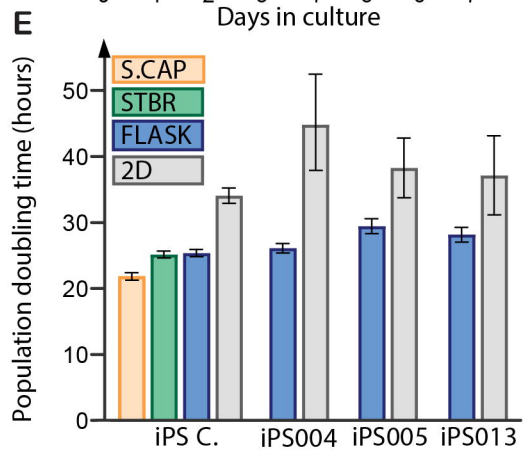
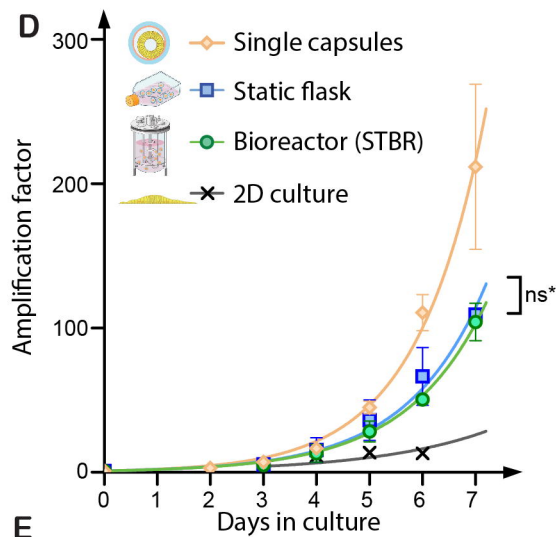
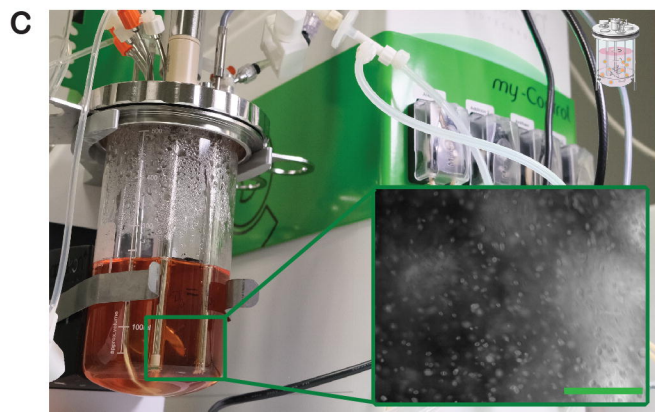
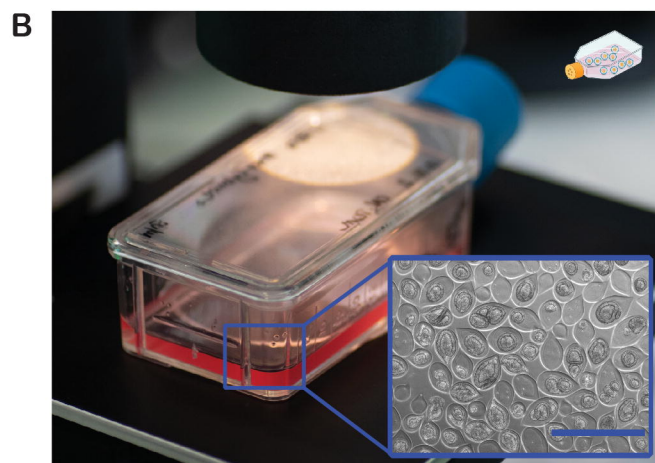
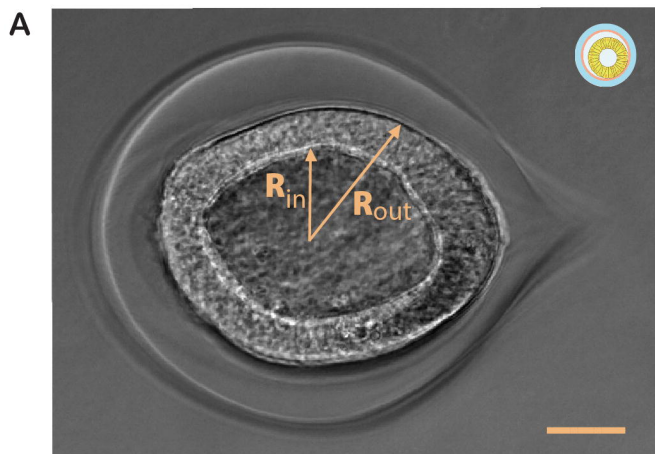
940

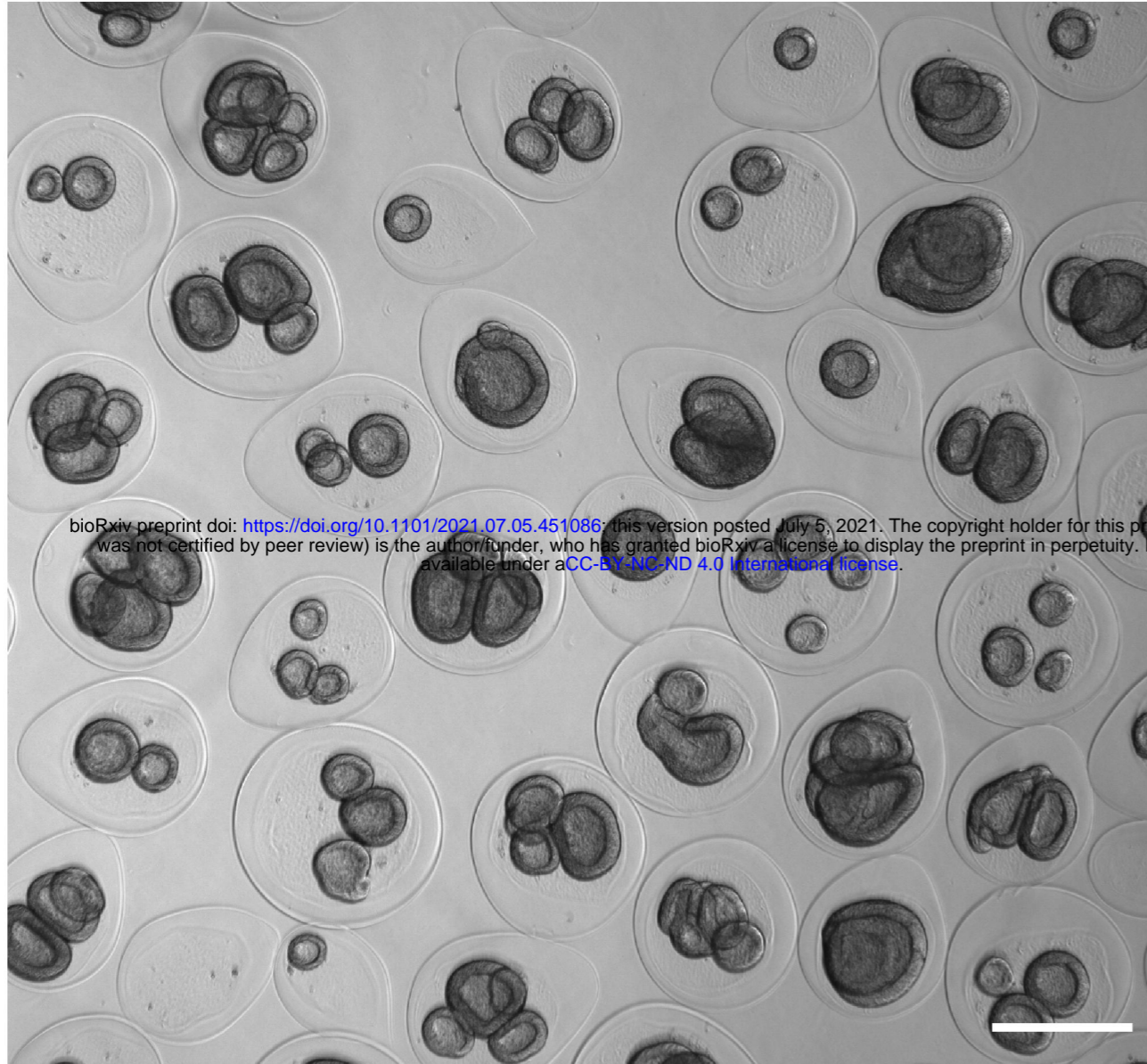
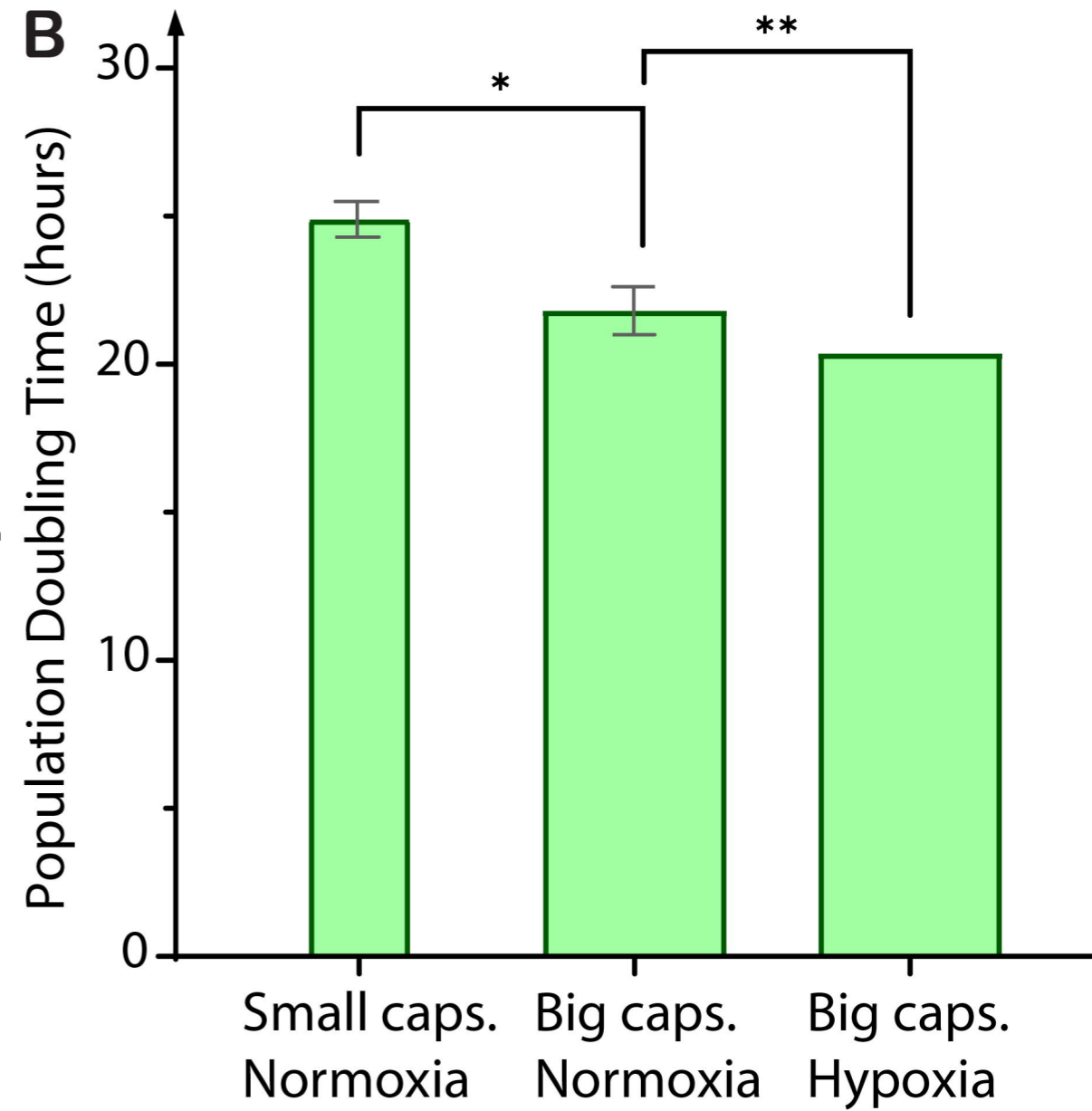
Antibodies used for immunostaining and microscopy	
OCT 3/4 mouse IgG2b (1/200)	Santa Cruz Biotechnology sc-5279 E1818
SOX2 Rabbit Polyclonal (1/1000)	Sigma Aldrich AB5603 3153252
Secondary Donkey anti-mouse IgG H+L Alexa Fluor Plus 488 1/500	Thermo/Invitrogen A32766 TF271737A
Secondary donkey anti-rabbit IgG H+L Alexa Fluor Plus 555 1/500	Thermo/Invitrogen A32794 TH271030
Phalloidin Alexa Fluor 647 at 1:500	Thermo A22287 2015553
Hoechst 33342 at 1:1000	









A**B****C****D**